# $G_{\alpha q}$-containing G proteins regulate B cell selection and survival and are required to prevent B cell–dependent autoimmunity

Ravi S. Misra,[1] Guixiu Shi,[2] Miguel E. Moreno-Garcia,[3] Anil Thankappan,[4] Michael Tighe,[4] Betty Mousseau,[1] Kim Kusser,[1] Shirly Becker-Herman,[3] Kelly L. Hudkins,[5] Robert Dunn,[7] Marilyn R. Kehry,[7] Thi-Sau Migone,[8] Ann Marshak-Rothstein,[9] Melvin Simon,[10] Troy D. Randall,[1] Charles E. Alpers,[5] Denny Liggitt,[6] David J. Rawlings,[3] and Frances E. Lund[1]

[1]Department of Medicine, Division of Allergy, Immunology, and Rheumatology, University of Rochester, Rochester, NY 14642
[2]Division of Rheumatology, State Key Laboratory of Biotherapy, West China Hospital, Sichuan University, Chengdu 610041, China
[3]Department of Pediatrics, University of Washington and Seattle Children's Research Institute, Seattle, WA 98101
[4]Trudeau Institute, Saranac Lake, NY 12983
[5]Department of Pathology and [6]Department of Comparative Medicine, University of Washington, Seattle, WA 98195
[7]Immunology, Biogen Idec, San Diego, CA 92122
[8]Clinical Immunology, Human Genome Sciences, Rockville, MD 20850
[9]Department of Medicine, Division of Rheumatology, University of Massachusetts Medical School, Worcester, MA 01655
[10]Department of Pharmacology, University of California, San Diego, School of Medicine, La Jolla, CA 92093

**Survival of mature B cells is regulated by B cell receptor and BAFFR-dependent signals. We show that B cells from mice lacking the $G_{\alpha q}$ subunit of trimeric G proteins (*Gnaq*$^{-/-}$ mice) have an intrinsic survival advantage over normal B cells, even in the absence of BAFF. *Gnaq*$^{-/-}$ B cells develop normally in the bone marrow but inappropriately survive peripheral tolerance checkpoints, leading to the accumulation of transitional, marginal zone, and follicular B cells, many of which are autoreactive. *Gnaq*$^{-/-}$ chimeric mice rapidly develop arthritis as well as other manifestations of systemic autoimmune disease. Importantly, we demonstrate that the development of the autoreactive B cell compartment is the result of an intrinsic defect in *Gnaq*$^{-/-}$ B cells, resulting in the aberrant activation of the prosurvival factor Akt. Together, these data show for the first time that signaling through trimeric G proteins is critically important for maintaining control of peripheral B cell tolerance induction and repressing autoimmunity.**

CORRESPONDENCE
Frances Lund:
frances_lund@urmc.rochester.edu
OR
David Rawlings:
drawling@u.washington.edu

Abbreviations used: Ab, antibody; ANA, anti-nuclear Ab; EdU, 5-ethynyl-2′-deoxyuridine; FOB, follicular B cell; GC, germinal center; GPCR, G protein–coupled receptor; MZ, marginal zone; PNA, peanut agglutinin.

Autoreactive B cells significantly contribute to the morbidity and mortality associated with many autoimmune diseases (Manjarrez-Orduño et al., 2009). B cell tolerance is normally controlled at several checkpoints in the BM and periphery (Goodnow, 2007). In the periphery, BCR- and BAFFR-dependent signals are required for the differentiation of immature transitional B cells into mature B cells and the continued maintenance of mature B cells (Cancro, 2009). B cells that express BCRs with intermediate affinity for autoantigens are less competitive than nonautoreactive B cells for access to the survival niches in the spleen and are eliminated at the transitional T1 stage of development (Lesley et al., 2004; Thien et al., 2004). However, in the presence of excess BAFF (also known as BLyS), autoreactive B cells can pass the T1 checkpoint and enter the mature B cell pool (Thien et al., 2004). Thus, the appropriate survival and selection of B cells in the periphery appears to be dependent on a dynamic integration of BAFFR and BCR signals.

Engagement of either the BCR or BAFFR alone is insufficient to maintain mature B cell survival in the periphery (Cancro, 2009), as BCR signaling is required to sustain NF-κB–dependent BAFFR signaling (Stadanlick et al., 2008). In addition to the NF-κB–dependent cross talk between BAFFR and the BCR, both receptors can also activate PI3K (Fruman and

R.S. Misra and G. Shi contributed equally to this paper.



The Rockefeller University Press $30.00
J. Exp. Med. Vol. 207 No. 8 1775-1789
www.jem.org/cgi/doi/10.1084/jem.20092735

Bismuth, 2009) and its downstream target Akt (Pogue et al., 2000; Patke et al., 2006), a serine threonine kinase which functions as a prosurvival factor in many cell types (Manning and Cantley, 2007). One recent study showed that BCR-dependent survival of mature B cells is highly dependent on PI3K (Srinivasan et al., 2009), and another study showed that activation of the PI3K pathway can rescue normally anergic autoreactive B cells (Browne et al., 2009). The PI3K–Akt signaling pathway is also engaged by activation of seven transmembrane-spanning G protein–coupled receptors (GPCRs; Yanamadala et al., 2009). GPCRs associate with heterotrimeric G proteins in their GDP-bound state (Wettschureck et al., 2004). Upon ligand binding to the GPCR, GDP is exchanged for GTP, which causes G protein release and the disassociation of the GTP-bound α subunit and the βγ dimer. Signal transduction is mediated by both the GTP-bound α subunit and the βγ dimer, but specialization and diversification of the response is often mediated by the GTP-bound α subunits (Wettschureck et al., 2004). There are 16 α subunits that fall into four classes, $G_{\alpha i}$, $G_{\alpha s}$, $G_{\alpha q/11}$, and $G_{12/13}$, based on their downstream signaling targets. PI3K can be activated by the βγ dimers released from $G_{\alpha i}$-coupled receptors (Wettschureck et al., 2004). In contrast, $G_{\alpha q}$, a member of the $G_{\alpha q/11}$ family, normally inhibits PI3K activation and prevents activation of Akt (Harris et al., 2006). In cardiomyocytes, Akt activation and cell survival is enhanced when the amount of active GTP-bound $G_{\alpha q}$ is low (Howes et al., 2006). However, when the amount of active $G_{\alpha q}$ is increased in cardiomyocytes, Akt activity is inhibited (Ballou et al., 2003) and survival of the cells upon stimulation is reduced (Howes et al., 2003). Examination of cardiomyocytes from transgenic mice expressing $G_{\alpha q}$ in the cardiomyocytes indicated that the level of cardiomyocyte apoptosis correlated directly with the amount of active $G_{\alpha q}$ expressed in the cells (Adams et al., 1998). Likewise, increased expression levels of $G_{\alpha q}$ are associated with changes in cardiomyocyte survival and in the development of cardiac disease in patients (Liggett et al., 2007; Frey et al., 2008). Together, these data suggest that one major function of $G_{\alpha q}$ is to suppress the PI3K/Akt signaling axis and cell survival. Surprisingly, despite that fact $G_{\alpha q}$ is expressed ubiquitously in B cells and myeloid cells (Wilkie et al., 1991), nothing is known regarding the requirement for $G_{\alpha q}$-containing G proteins in regulating Akt activity or hematopoietic cell survival.

In this paper, we show that $G_{\alpha q}$ regulates peripheral B cell tolerance by suppressing the survival and selection of autoreactive B cells. In the absence of $G_{\alpha q}$, B cells constitutively express higher levels of activated Akt and preferentially survive BCR-induced cell death signals and BAFF withdrawal in vitro and in vivo. Most importantly, $G_{\alpha q}$-deficient mice rapidly develop an autoreactive B cell repertoire and systemic autoimmunity. Together, these data show that $G_{\alpha q}$-containing G proteins, working in concert with the BCR and BAFFR signaling networks, regulate B cell development and peripheral tolerance induction. In addition, the data provide the first example of G protein–dependent suppression of B cell–mediated autoimmunity.

## RESULTS

### $G_{\alpha q}$ regulates peripheral B cell homeostasis

Our laboratory previously showed that $G_{\alpha q}$ regulates the in vitro chemotaxis of BM-derived neutrophils and DCs (Shi et al., 2007). Based on these data, we wanted to test whether $G_{\alpha q}$ was also required for B cell migration. However, mice lacking $G_{\alpha q}$ (*Gnaq*$^{-/-}$ mice) are difficult to study as they are born runted and exhibit motor defects (Offermanns et al., 1997). Therefore, to analyze the role of $G_{\alpha q}$ specifically in immune cells, we generated BM chimeric mice by reconstituting lethally irradiated C57BL/6J recipient mice with either C57BL/6 BM (WT chimeras) or *Gnaq*$^{-/-}$ BM (*Gnaq*$^{-/-}$ chimeras). To determine whether $G_{\alpha q}$ expressed by hematopoietic cells was required for the positioning of B and T cells within lymphoid tissues, we examined the splenic architecture of *Gnaq*$^{-/-}$ and WT chimeras. Using antibodies (Abs) to B220, CD21, and CD90.2 (Thy1.2) we identified B220$^{+}$ B follicles containing CD21$^{+}$ follicular DC networks and CD90.2$^{+}$ T cell zones in the spleens of WT and *Gnaq*$^{-/-}$ chimeras (Fig. 1 A). However, the numbers of CD21$^{hi}$ B cells within the splenic marginal zone (MZ) appeared to be increased in the *Gnaq*$^{-/-}$ chimeras (Fig. 1 A). To address whether this alteration was a result of changes in the migratory potential of the *Gnaq*$^{-/-}$ B cells, we performed chemotaxis assays using spleen cells from WT and *Gnaq*$^{-/-}$ chimeras. We found that the *Gnaq*$^{-/-}$ B cells migrated normally to CXCL13, CXCL12, CCL19, and S1P (Fig. 1 B). Furthermore, upon transfer of purified WT and *Gnaq*$^{-/-}$ B cells to intact hosts, we found that the *Gnaq*$^{-/-}$ B cells migrated to both the B cell follicle and MZ of the spleen (Fig. 1 C). Therefore, the expansion of the MZ in the *Gnaq*$^{-/-}$ chimeras did not appear to be a result of overt changes in the migratory capacity of the *Gnaq*$^{-/-}$ B cells.

Previous experiments indicated that $G_{\alpha i}$-containing G proteins regulate BCR signaling, B cell activation, and partitioning of B cells between the follicular and MZB cell subsets (Dalwadi et al., 2003). We therefore tested whether $G_{\alpha q}$, like $G_{\alpha i}$, regulates B cell development or maturation in the BM of chimeric mice (Fig. S1 A). We found that the total numbers of B220$^{+}$ B cells in the BM of both groups of chimeras were equivalent (Fig. 1 D). Likewise, the absolute numbers of pro–B, pre–B (large and small), and immature B cells were indistinguishable between WT and *Gnaq*$^{-/-}$ chimeras (Fig. 1 D).

Next, we examined peripheral B cell development using CD93, IgM, and CD23 to identify the T1, T2, and T3 subsets in the spleens of *Gnaq*$^{-/-}$ and WT chimeras (Fig. S1 B). We found no differences between the numbers of T2 and T3 cells in the spleens of *Gnaq*$^{-/-}$ and WT chimeras (Fig. 1 E). However, we reproducibly observed an increase in the percentage (Fig. S1 B) and number (Fig. 1 E) of T1 cells in the spleens of *Gnaq*$^{-/-}$ chimeras. Interestingly, the percentages (Fig. S1 C) and absolute numbers (Fig. 1 E) of CD19$^{+}$ splenic B cells, CD19$^{+}$CD21$^{hi}$CD23$^{lo}$ MZ B cells (MZBs), and CD19$^{+}$CD21$^{lo}$CD23$^{hi}$ follicular B cells (FOBs) were higher in the *Gnaq*$^{-/-}$ chimeras compared with WT chimeras. Likewise, the percentage of CD21$^{hi}$ B cells expressing the MZB cell marker CD1d$^{hi}$ was also significantly elevated in

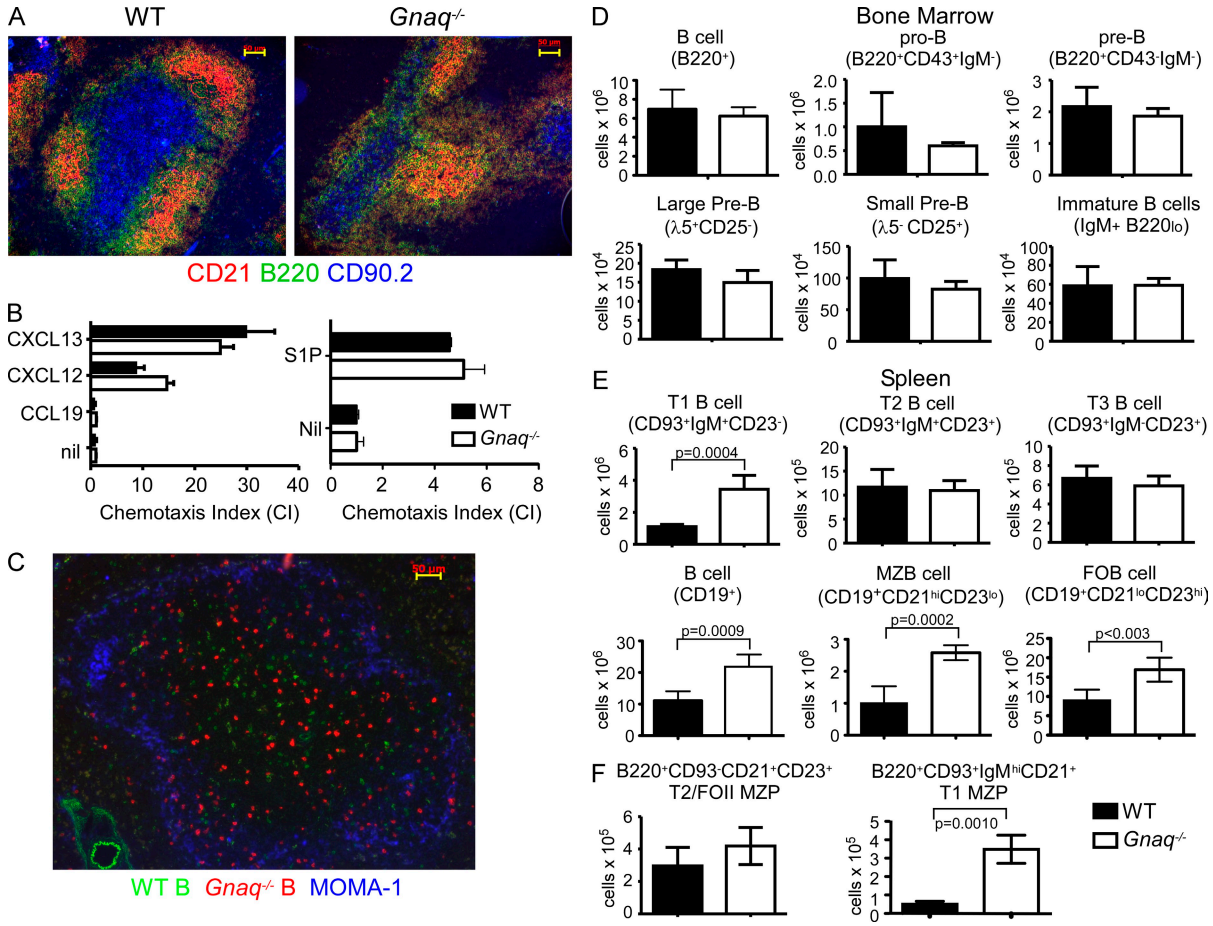


**Figure 1. Altered B cell homeostasis in $G_{\alpha q}$-deficient chimeras.** (A) Frozen sections of WT and *Gnaq*$^{-/-}$ BM chimera spleens were stained with anti-CD90.2 to identify T cell zones (blue), anti-B220 to identify B cell follicles (green), and anti-CD21 (red) to identify follicular DC networks in the B cell follicle and CD21$^{hi}$ B cells within the MZ. (B) Total B cells were isolated from WT and *Gnaq*$^{-/-}$ chimera spleens and analyzed in in vitro chemotaxis assays using 300 ng/ml CXCL12, 500 ng/ml CXCL13, 400 ng/ml CCL19, or 10 nM S1P as chemoattractants. Data are presented as the mean ± SD of triplicate wells. (C) Splenic B cells from CD45.1$^{+}$ WT and CD45.2$^{+}$ *Gnaq*$^{-/-}$ chimeras were purified. WT B cells were labeled with biotin and equivalent numbers of WT and *Gnaq*$^{-/-}$ B cells were transferred into CD45.1$^{+}$ hosts. Frozen sections were prepared from spleens 18 h after transfer and stained with SA-488 to visualize the transferred WT B cells (green), anti-CD45.2 to visualize transferred *Gnaq*$^{-/-}$ B cells (red), and anti–MOMA-1 (blue) to visualize the MZ. Bars, 50 µm. (D–F) BM and spleens were harvested from *Gnaq*$^{-/-}$ and WT chimeras, stained with the indicated Abs to identify B cell subsets, and then analyzed by flow cytometry. (D) The absolute numbers of total BM B cells, pro–B, pre–B (large and small), and immature B cells were determined. (E) The numbers of T1, T2, and T3 transitional B cells and the numbers of total splenic B cells, FOB cells, and MZB cells were determined. (F) The numbers of splenic T2/FOII MZB precursors and T1 MZB precursors were determined. Data shown are the mean ± SD of five mice/group. P-values were determined using an unpaired Student's *t* test. Data in all panels are representative of three or more independent experiments.

the spleens of *Gnaq*$^{-/-}$ chimeras (Fig. S1 D). However, inconsistent with the phenotype of conventional MZB cells, ∼50% of the CD21$^{hi}$CD23$^{lo}$ MZ-like B cells found in the spleens of the *Gnaq*$^{-/-}$ chimeras also expressed high levels of IgD (Fig. S1 E).

To determine whether the expansion of MZ-like B cells in the *Gnaq*$^{-/-}$ chimera spleens was the result of changes in the number of MZB precursors, we first examined the B220$^{+}$CD93$^{-}$CD23$^{hi}$CD21$^{hi}$ MZB cell precursors that are thought to arise from the T2 or FOII population (Srivastava et al., 2005; Cariappa et al., 2007). We found no difference between the percentages (Fig. S1 F) or numbers (Fig. 1 F) of these cells in spleens of *Gnaq*$^{-/-}$ and WT chimeras. We next examined the MZB precursors (B220$^{+}$CD93$^{+}$CD23$^{-}$IgM$^{hi}$ CD21$^{hi}$) found in the T1 population (Carey et al., 2008). Interestingly, both the frequency (Fig. S1 G) and total number (Fig. 1 F) of the T1-derived MZB precursors were significantly elevated in the spleens of *Gnaq*$^{-/-}$ chimeras. Collectively, the data suggest that $G_{\alpha q}$ is not required for B cell development in the BM. However, $G_{\alpha q}$ does modulate peripheral B cell development and appears to control the numbers of T1 cells, T1-derived MZB cell precursors, and mature MZB and FOB cells.

### $G_{\alpha q}$ regulates B cell survival in vitro

Given the alterations in splenic B cell homeostasis in *Gnaq*$^{-/-}$ chimeras, we hypothesized that $G_{\alpha q}$ may regulate B cell expansion or survival. To test this hypothesis, we cultured splenic WT and *Gnaq*$^{-/-}$ B cells in media alone or with

increasing amounts of anti-IgM F(ab′)$_2$ for 48 h, pulsed the cells with $^3$H-thymidine for 5 h, and measured thymidine incorporation. No major differences in DNA replication were observed between unstimulated and anti-IgM–stimulated *Gnaq*$^{-/-}$ and WT B cells (Fig. 2 A). Likewise, we did not observe any differences in DNA replication between *Gnaq*$^{-/-}$ and WT B cells stimulated with agonistic anti-CD40 Abs (Fig. 2 B). However, *Gnaq*$^{-/-}$ B cells did proliferate more strongly (~30% increase) in response to LPS than their WT counterparts (Fig. 2 C), suggesting that either a higher proportion of *Gnaq*$^{-/-}$ B cells are responsive to LPS or that *Gnaq*$^{-/-}$ B cells are hyperresponsive to TLR4 ligands.

Because the loss of $G_{\alpha q}$ only modestly affected the in vitro proliferative responses of splenic B cells, we next examined whether $G_{\alpha q}$ regulates B cell survival. We cultured purified WT or *Gnaq*$^{-/-}$ B cells in media alone or with anti-IgM F(ab′)$_2$ and monitored viability. Surprisingly, a larger fraction of *Gnaq*$^{-/-}$ B cells remained viable in both unstimulated and anti-IgM–stimulated cultures (Fig. 2 D), suggesting that $G_{\alpha q}$ plays a role in regulating the in vitro survival of mature B cells. To address whether $G_{\alpha q}$ also modulates immature B cell survival, we sort purified T1 B cells and T2/T3 B cells from the spleens of WT and *Gnaq*$^{-/-}$ chimeras, cultured the cells in media alone or with anti-IgM F(ab′)$_2$ for 18 h, and measured B cell viability. As expected (Su and Rawlings, 2002), WT T1 B cells died rapidly after anti-Ig stimulation (Fig. 2 E), whereas WT T2/T3 B cells were largely resistant to anti-IgM–induced cell death (Fig. 2 F). Interestingly, significantly more of the *Gnaq*$^{-/-}$ T1 (Fig. 2 E) and T2/T3 B cells (Fig. 2 F) survived the culture period, regardless of whether the B cells were stimulated with anti-IgM or cultured in media alone. Thus, *Gnaq*$^{-/-}$ B cells survive in vitro in higher numbers than WT B cells at all stages of transitional and mature B cell development.

## Increased activation of BCR-mediated signaling in *Gnaq*$^{-/-}$ B cells

GTP-bound $G_{\alpha q}$ is reported to suppress activation of PI3K and Akt in nonhematopoietic cells (Bommakanti et al., 2000; Ballou et al., 2003). Given the enhanced in vitro survival of *Gnaq*$^{-/-}$ B cells, we next tested whether the loss of $G_{\alpha q}$ leads to enhanced Akt activation in B cells. We purified splenic B cells from WT and *Gnaq*$^{-/-}$ chimeras, stimulated the cells with anti-IgM F(ab′)$_2$ for 0–30 min, prepared total protein lysates, and performed Western blot analysis. We found that the basal levels of phospho-Akt (p-Ser473) were higher in *Gnaq*$^{-/-}$ B cells than in WT B cells (Fig. 3 A). Furthermore, upon anti-IgM stimulation phospho-Akt levels increased more rapidly in *Gnaq*$^{-/-}$ B cells (Fig. 3 A), and the peak amount of phospho-Akt was higher in the anti-IgM–stimulated *Gnaq*$^{-/-}$ B cells than in the anti-Ig–stimulated WT B cells (Fig. 3 B). We also found that the levels of phosphorylated PLCγ2 (Y759) and Erk were significantly increased in the anti-IgM–stimulated *Gnaq*$^{-/-}$ B cells relative to the WT B cells (Fig. 3, A and C). Consistent with these results, we noted that several protein species were hyperphosphorylated on either tyrosine (Fig. S2 A) or serine (Fig. S2 B) in the unstimulated *Gnaq*$^{-/-}$ B cells relative to the WT B cells and were further phosphorylated as early as 1 min after anti-IgM stimulation. Thus, several signaling substrates, including Akt, are hyperphosphorylated in *Gnaq*$^{-/-}$ B cells both before and after BCR ligation.

To address whether the increased Akt phosphorylation observed in the anti-IgM–stimulated splenic *Gnaq*$^{-/-}$ B cells

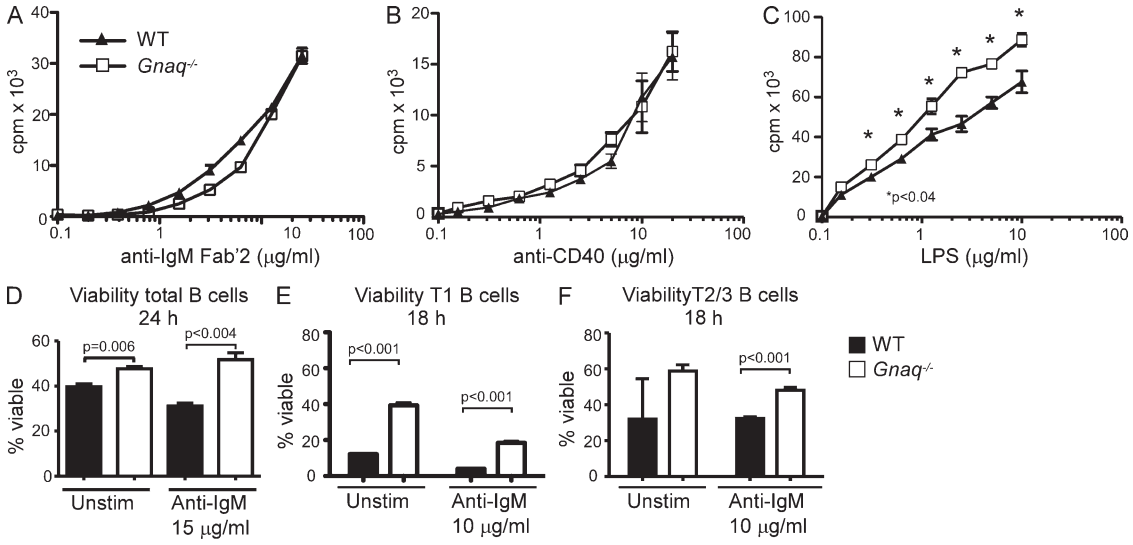


**Figure 2. $G_{\alpha q}$-deficient B cells exhibit a prosurvival phenotype in vitro.** (A–C) WT or *Gnaq*$^{-/-}$ splenic B cells were stimulated with 0–25 μg/ml anti-IgM F(ab′)$_2$ (A), 0–40 μg/ml anti-CD40 (B), or 0–10 μg/ml LPS (C) for 48 h and proliferative responses were measured by $^3$H-thymidine incorporation after a 5-h pulse. Results represent the mean ± SD of triplicate cultures. (D–F) Purified total splenic B cells (D), sort-purified B220$^+$CD93$^+$CD23$^-$ T1 B cells (E), or sort-purified B220$^+$CD93$^+$CD23$^+$ T2/T3 B cells (F) were cultured in media alone or stimulated with 10–15 μg/ml anti-IgM F(ab′)$_2$ for 18–24 h. Viability was measured by staining with propidium iodide. Data are shown as the mean ± SD of triplicate cultures. P-values were determined using an unpaired Student's *t* test. Data in all panels are representative of three independent experiments.

was a result of the presence of more MZB cells in the *Gnaq*$^{-/-}$ spleens, we assessed phospho-Akt levels in CD43$^{neg}$ naive B cells and enriched populations of FOB and MZB cells. As expected, phospho-Akt levels were constitutively elevated in naive CD43$^{neg}$ *Gnaq*$^{-/-}$ B cells and more rapidly reached peak levels after anti-IgM stimulation (Fig. 3 D). In contrast, the phospho-Akt levels in the enriched FOB cells were equivalent between the WT and *Gnaq*$^{-/-}$ B cells both before and after anti-IgM stimulation (Fig. 3 D). However, phospho-Akt levels were constitutively elevated in the *Gnaq*$^{-/-}$ MZB cells relative to the WT MZB cells (Fig. 3 D). Furthermore, phospho-Akt levels increased to peak levels more rapidly and were sustained for extended periods of time after BCR stimulation in the *Gnaq*$^{-/-}$ MZB cells (Fig. 3 D). Together, these data suggest that Akt activation after BCR engagement is specifically enhanced in *Gnaq*$^{-/-}$ MZB cells.

### *Gnaq*$^{-/-}$ B cells outcompete WT B cells for access to splenic niches in vivo

Collectively, our data suggested that *Gnaq*$^{-/-}$ B cells may survive better than WT B cells in vivo. To test this, we transferred equivalent numbers of splenic B cells from WT or *Gnaq*$^{-/-}$ chimeras (CD45.2$^+$) into intact congenic CD45.1$^+$ WT hosts (Fig. 4 A). At various time points after transfer, we enumerated donor CD45.2$^+$ B cells in the spleen by FACS. As shown in Fig. 4 (B and C), the percentages and numbers of donor *Gnaq*$^{-/-}$ B cells recovered at 1 wk after transfer were significantly higher compared with those found in recipients receiving WT B cells. At days 14 and 21 after transfer, very few of the transferred WT B cells could be found in the congenic hosts (Fig. 4 B). However, the transferred *Gnaq*$^{-/-}$ B cells were easily detectable and present at 10-fold higher frequencies and numbers than the WT B cells (Fig. 4, B and C). Thus, the data suggested that *Gnaq*$^{-/-}$ B cells survive longer in vivo than WT B cells.

Next, to address whether the *Gnaq*$^{-/-}$ B cells are more fit to survive than WT B cells, we prepared mixed BM chimeras by transferring equivalent numbers of WT (CD45.1$^+$) and *Gnaq*$^{-/-}$ (CD45.2$^+$) BM cells into lethally irradiated WT CD45.1$^+$ recipient mice (Fig. 4 D) and determined the relative composition of the splenic B cells after reconstitution. We found that the ratio of *Gnaq*$^{-/-}$ B cells to WT B cells was already significantly increased by 1 mo after reconstitution (Fig. 4 E). Furthermore, by 8 wk after reconstitution the ratio of *Gnaq*$^{-/-}$ to WT B cells was 4:1, and within 6 mo the ratio was 19:1 in favor of the *Gnaq*$^{-/-}$ B cells (Fig. 4 E). We found that the FOB and MZB compartments were both skewed in favor of the *Gnaq*$^{-/-}$ B cells at 8 wk after reconstitution; however, the MZB cell compartment was more highly skewed than the FOB compartment toward the *Gnaq*$^{-/-}$ B cells (Fig. 4 F). Likewise, all of the transitional B cells in the spleen were already highly skewed toward the *Gnaq*$^{-/-}$ B cells by 8 wk after reconstitution (Fig. 4 F). Interestingly, the T1 MZB precursor population was almost entirely derived from the *Gnaq*$^{-/-}$ B cells within 8 wk after reconstitution (ratio of 20:1; Fig. 4 F). The skewing of the peripheral B cell compartments toward *Gnaq*$^{-/-}$ B cells was not a result of changes in the output of B cell progenitors from the BM, as the ratio of *Gnaq*$^{-/-}$ to WT immature B cells in the BM (fraction E) remained very close to 1:1 at 8 wk after reconstitution (Fig. 4 F). However, the ratio of *Gnaq*$^{-/-}$ to WT B220$^+$CD93$^+$IgM$^+$CD23$^+$ transitional B cells in the BM (Lindsley et al., 2007) increased slightly (~2.0) and the recirculating mature B cells in the BM were highly skewed toward the *Gnaq*$^{-/-}$ genotype (10:1 ratio; Fig. 4 F).

Finally, to evaluate whether the increase in *Gnaq*$^{-/-}$ B cells relative to WT B cells in the spleen of the mixed chimeric mice was the result of increased proliferation of the *Gnaq*$^{-/-}$ B cells, we injected the 50:50 BM chimeras with 5-ethynyl-2′-deoxyuridine (EdU) at 8 wk after reconstitution and then

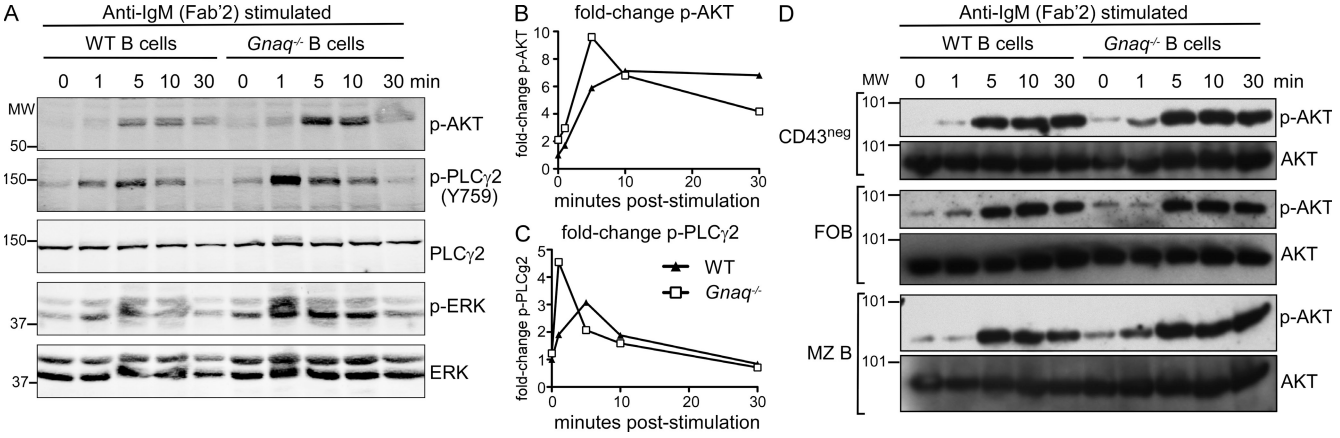


**Figure 3. $G_{\alpha q}$-deficient B cells are hyperresponsive to BCR triggering.** (A–D) Splenic B cells from *Gnaq*$^{-/-}$ and WT chimeras were stimulated with anti-IgM F(ab′)$_2$ for 0–30 min. Protein lysates were prepared from negatively selected total B cells (A and D) or from enriched FOB and MZB cells (D) and then analyzed by Western blotting. Akt (p-Ser473), PLCγ2, and Erk were probed with phospho-specific Abs and protein-specific Abs. Li-COR quantitative densitometry was used to determine the fold changes in phospho-Akt (B) and phospho-PLCγ2 (C). The ratios of phospho-specific proteins versus total ERK or PLCγ2 were obtained and data were normalized to WT B cells at time 0 (set as 1). Data in all panels are representative of two independent experiments.

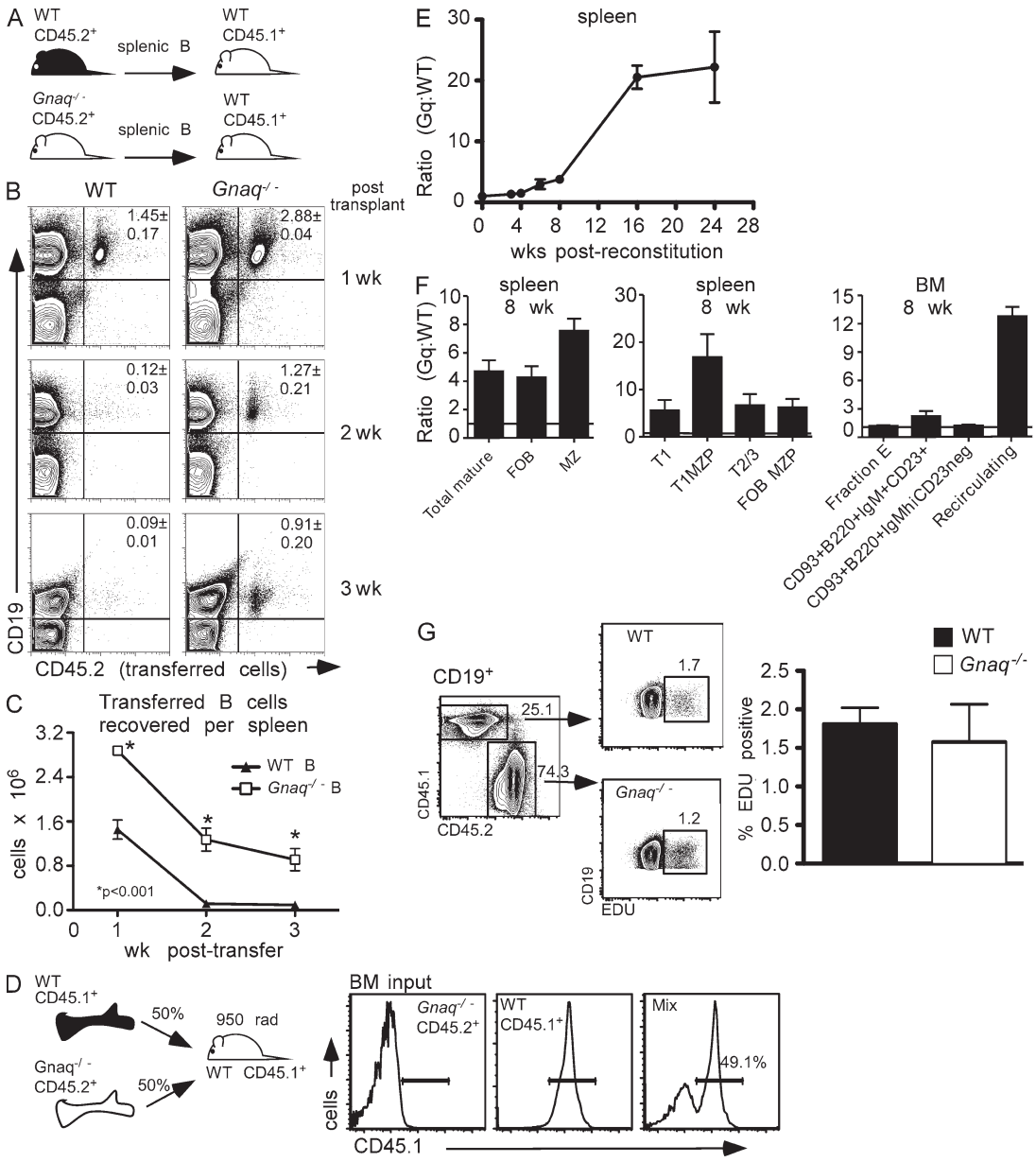


**Figure 4. $G_{\alpha q}$-deficient B cells have a competitive survival advantage over WT B cells in vivo.** (A–C) Splenic B cells were purified from WT and *Gnaq*$^{-/-}$ chimeras (CD45.2$^+$) and transferred i.v. into CD45.1$^+$ WT hosts (2.5 × 10$^7$ cells/host). (B) Spleen cells from recipient mice were harvested at 1–3 wk after transfer and analyzed by flow cytometry to identify donor B cells. Representative dot plots and the mean percentage ± SD of cells of donor origin are shown. (C) The number of donor B cells recovered per recipient spleen was determined and is shown as the mean ± SD ($n$ = 3–5 mice/group/time point). Data are representative of two independent experiments. (D–G) Lethally irradiated CD45.1$^+$ WT mice were reconstituted with a mixture of BM consisting of 50% *Gnaq*$^{-/-}$ (CD45.2$^+$) BM and 50% WT (CD45.1$^+$) BM. (E) Splenic B cells were collected from the 50:50 BM chimeras and flow cytometry was used to identify WT and *Gnaq*$^{-/-}$ B cells. Data are presented as the ratio of *Gnaq*$^{-/-}$ to WT B cells (percentage of *Gnaq*$^{-/-}$ B cells divided by percentage of WT B cells) at each time point and are shown as the mean ± SD from five mice per group. Data are representative of more than three independent experiments. (F) BM and spleen were collected from the 50:50 BM chimeras at 2 mo after reconstitution, and the ratio of *Gnaq*$^{-/-}$ to WT B cells was determined as described in E. Splenic B cells were subdivided into total mature (B220$^+$CD93$^-$), FOB (B220$^+$CD21$^{lo}$CD23$^{hi}$), MZB (B220$^+$CD21$^{hi}$CD23$^{lo}$), T1 (B220$^+$CD93$^+$CD23$^-$), T2/T3 (B220$^+$CD93$^+$CD23$^+$), T1 MZB precursors (B220$^+$CD93$^+$IgM$^{hi}$CD21$^{hi}$), and T2/FOII MZB precursors (B220$^+$CD93$^-$CD21$^{hi}$CD23$^{hi}$). B cells in the BM were subdivided into immature (fraction E) B cells (B220$^+$CD93$^+$IgM$^+$), transitional (B220$^+$CD93$^+$IgM$^{hi}$CD23$^+$), and recirculating (B220$^{hi}$IgM$^+$IgD$^+$). Data are shown as the mean ± SD of four to five mice/group. (G) 50:50 BM chimeras (2 mo after reconstitution) were injected with EdU twice over a 12-h period. Spleen cells were isolated at 18 h, stained with Abs to CD19 and CD45.2 and the EdU detection reagent, and then analyzed by flow cytometry. Representative FACS plots are shown and the percentage of B cells of each genotype that incorporated EdU is provided. Data shown are the mean ± SD of five mice. Data in D–G are representative of two independent experiments.

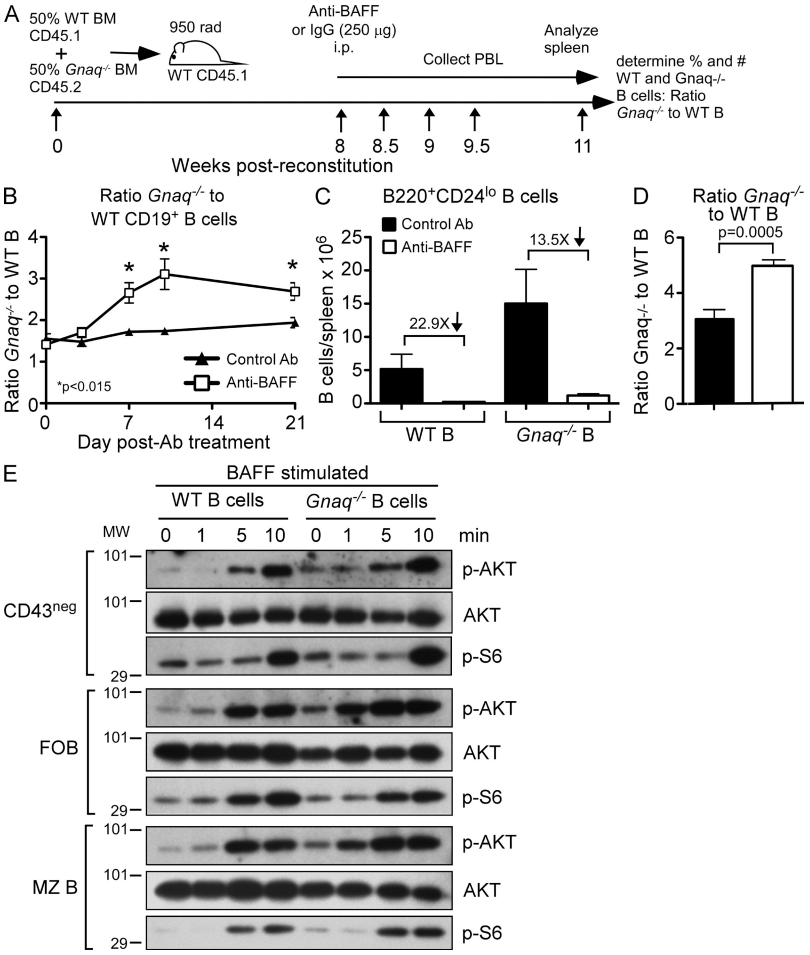


**Figure 5. *Gnaq*$^{-/-}$ B cells are more resistant to BAFF neutralization in vivo and are more sensitive to BAFF stimulation in vitro.** (A–D) 50:50 mixed BM chimeras were generated using *Gnaq*$^{-/-}$ BM (CD45.2$^+$) and WT (CD45.1$^+$) BM. 8 wk after reconstitution, chimeric animals were injected i.p. with a blocking Ab to BAFF/BLyS (clone 10F4) or an isotype control Ab. (B) Peripheral blood samples were collected from Ab-treated chimeric animals between 7 and 21 d and flow cytometry was used to identify the percentage of B cells that were of WT or *Gnaq*$^{-/-}$ origin. Data are shown as the ratio (±SEM) of *Gnaq*$^{-/-}$ to WT B cells (percentage of *Gnaq*$^{-/-}$ B cells divided by percentage of WT B cells; $n = 5–10$ mice). P-values were determined using an unpaired Student's *t* test. (C) Spleen cells from Ab-treated chimeras were isolated, enumerated, and analyzed by flow cytometry at 21 d after treatment. The numbers of mature splenic B cells (B220$^+$CD24$^{lo}$) of WT and *Gnaq*$^{-/-}$ origin were determined and are reported as the mean ± SD of five mice/group. The fold depletion caused by BAFF neutralization is shown above the bar graphs. (D) The ratio of *Gnaq*$^{-/-}$ to WT B cells in the spleen was calculated (percentage of *Gnaq*$^{-/-}$ B cells divided by percentage of WT B cells) and is shown as the mean ± SD. P-values were determined using an unpaired Student's *t* test. Data in A–D are representative of three independent experiments. (E) Splenic CD43$^{neg}$ naive B cells were isolated from *Gnaq*$^{-/-}$ and WT chimeras and enriched for CD21$^{lo}$ FOB and CD21$^{hi}$ MZB cells. The total or enriched B cell subsets were cultured in BAFF-free media overnight. Live cells were recovered from the cultures and stimulated with recombinant BAFF for 0–10 min. Protein lysates were prepared and analyzed by Western blotting. Phospho-Akt (p-Ser473), total Akt, and phospho-S6 ribosomal protein were detected using phospho- and protein-specific Abs. Data in E is representative of two experiments.

determined the proportion of WT and *Gnaq*$^{-/-}$ B cells that proliferated in 18 h. As shown in Fig. 4 G, the percentage of replicating B cells was not significantly different between *Gnaq*$^{-/-}$ and WT B chimeras. Together, these data argue that the *Gnaq*$^{-/-}$ B cells are not overtly more proliferative than WT B cells but are able to efficiently outcompete WT B cells for access to or retention within peripheral survival niches.

### *Gnaq*$^{-/-}$ B cells are more resistant to BAFF withdrawal

Because *Gnaq*$^{-/-}$ B cells quickly outcompete WT B cells in the spleen, we next tested whether the *Gnaq*$^{-/-}$ B cells are less reliant on survival factors such as BAFF. We generated 50:50 mixed BM chimeras by transferring equal amounts of CD45.1$^+$ WT BM and CD45.2$^+$ *Gnaq*$^{-/-}$ BM to irradiated CD45.1 WT hosts. We treated the recipients with a neutralizing anti-BAFF or isotype control Ab 8 wk after reconstitution and then monitored WT and *Gnaq*$^{-/-}$ B cells in the peripheral blood and spleen over the next 3 wk (Fig. 5 A). We determined the percentage of B cells in peripheral blood that were either $G_{\alpha q}$ deficient or WT at each of the time points (Fig. S3 A) and then calculated the ratio of *Gnaq*$^{-/-}$ B cells to WT B cells. The ratio of peripheral blood *Gnaq*$^{-/-}$ B cells to WT B cells was ∼1.5 at 8 wk after reconstitution (Fig. 5 B), indicating that *Gnaq*$^{-/-}$ B cells were already overrepresented in the blood at this time. The ratio of *Gnaq*$^{-/-}$ B cells to WT B cells in peripheral blood modestly increased over the next 3 wk in the chimeras that were treated with the isotype control Ab (Fig. 5 B), which is consistent with the gradual takeover by *Gnaq*$^{-/-}$ B cells. However, the ratio of *Gnaq*$^{-/-}$ B cells to WT B cells increased even more rapidly in the anti-BAFF–treated chimeras (Fig. 5 B).

Next, we determined the percentage (Fig. S3 B) and number (Fig. 5 C) of mature WT (CD45.1$^+$) and *Gnaq*$^{-/-}$ (CD45.2$^+$) B cells present in the spleens of the mixed BM chimeras on day 21 after treatment. As expected, approximately three times more mature *Gnaq*$^{-/-}$ B cells were recovered relative to WT B cells in the control Ab–treated chimeras (Fig. 5 C). After BAFF blockade, we observed a significant reduction in the number of total mature B cells, regardless of genotype (Fig. 5 C). However, although the number of WT B cells decreased by 23-fold after anti-BAFF treatment, the number of *Gnaq*$^{-/-}$ B cells dropped by only 13.5-fold (Fig. 5 C). Furthermore, the ratio of splenic *Gnaq*$^{-/-}$ B cells to WT B cells increased from 3.1 in the control Ab–treated chimeras to 5.0

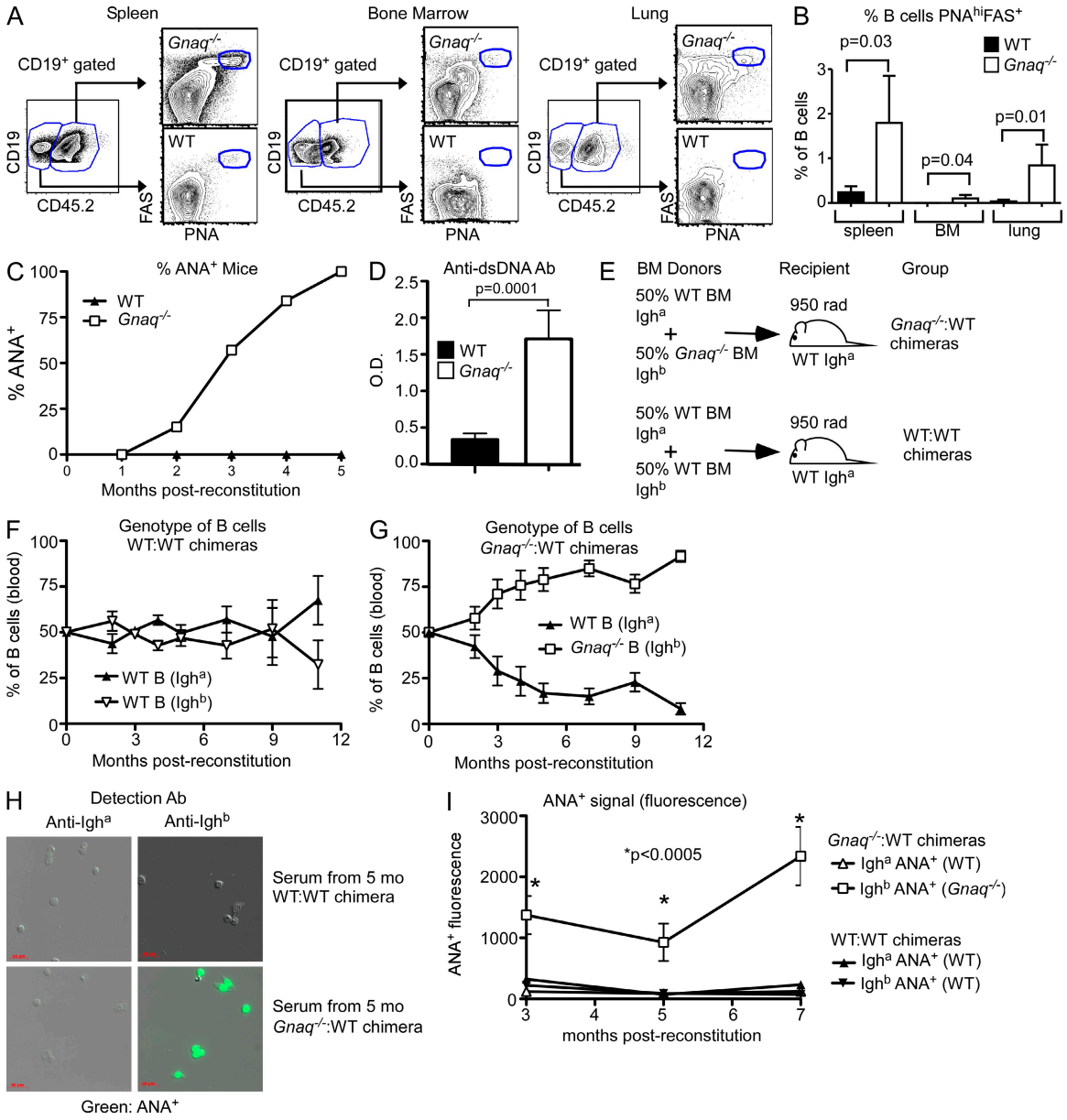


**Figure 6. $G_{\alpha q}$–deficient B cells display an activated phenotype and are intrinsically prone to develop autoreactive specificities.** (A and B) 50:50 mixed BM chimeras were generated using *Gnaq*$^{-/-}$ BM (CD45.2$^{+}$) and WT (CD45.1$^{+}$) BM. 11 wk after reconstitution, cells from BM, spleen, and lungs were harvested and B cells were analyzed by flow cytometry for expression of PNA and FAS. Representative FACs plots are shown (A) and the percentages of WT or *Gnaq*$^{-/-}$ B cells expressing a GC phenotype (PNA$^{hi}$FAS$^{+}$) were determined (B). Data are shown as the mean ± SD of four to five mice per time point. P-values were determined using an unpaired Student's *t* test. All data shown are representative of two independent experiments. (C) WT and *Gnaq*$^{-/-}$ BM chimeras were generated and aged for 5 mo. Serum samples were collected monthly. The presence of ANAs (ANA reactivity) in the serum (diluted 1:100) was then determined by fluorescence microscopy using fixed HepG2 cells. The data are shown as the percentage of animals with detectable ANAs in the serum ($n$ = 10 mice/group). (D) Serum samples were collected from female WT and *Gnaq*$^{-/-}$ chimeras at 9 mo after reconstitution. Samples were evaluated for reactivity to dsDNA by ELISA. Data shown are the mean OD ± SD from a 1/200 dilution of the serum samples. $n$ = 4–5 mice/group. P-values were determined using an unpaired *t* test. Data in panels C and D are representative of two or more independent experiments. (E–I) 50:50 mixed BM chimeras were made by reconstituting irradiated Igh$^{a}$ hosts with 50% WT BM (Igh$^{a}$ allotype) and 50% *Gnaq*$^{-/-}$ BM (Igh$^{b}$ allotype; referred to as *Gnaq*$^{-/-}$:WT chimeras) or with 50% WT BM (Igh$^{a}$ allotype) plus 50% WT BM (Igh$^{b}$ allotype; referred to as WT:WT chimeras). (F and G) Peripheral blood from the WT:WT (F) and *Gnaq*$^{-/-}$:WT (G) chimeras was analyzed by flow cytometry between 2 and 10 mo after reconstitution using allotype-specific Abs to identify the B cells of either WT or *Gnaq*$^{-/-}$ origin. Data are shown as the mean percentage of B cells of the different genotypes ± SD. $n$ = 10 mice/group. (H) Serum, isolated from WT:WT and *Gnaq*$^{-/-}$:WT chimeras at 5 mo after reconstitution, was incubated (1:100 dilution) with fixed HepG2 cells. ANA-reactive Abs were detected using allotype-specific Abs. Representative fluorescent images are shown. Bars, 50 µm. (I) The fluorescence signal detected from each serum sample was determined and shown as the mean fluorescent signal ± SD ($n$ = 9–10 mice/group). Data in E–I are representative of two independent experiments. P-values were determined using an unpaired Student's *t* test.

in the anti-BAFF–treated chimeras (Fig. 5 D). This change in the ratio of splenic *Gnaq*$^{-/-}$ B cells to WT B cells was not the result of an obvious difference in BAFFR expression levels between WT and *Gnaq*$^{-/-}$ B cells (Fig. S3, C and D). Thus, *Gnaq*$^{-/-}$ B cells are significantly more resistant to BAFF depletion than their WT counterparts.

BAFF signaling in B cells is reported to stimulate PI3K and induce activation of the Akt signaling pathway (Patke et al., 2006). Given the increase in constitutively phosphorylated Akt observed in the *Gnaq*$^{-/-}$ B cells and the increased resistance of these B cells to BAFF depletion, we evaluated whether *Gnaq*$^{-/-}$ B cells are more responsive to BAFF signals than their WT counterparts. We isolated splenic CD43$^{neg}$ naive B cells, FOB cells, and MZB cells from WT and *Gnaq*$^{-/-}$ chimeras. We cultured the cells overnight in the absence of BAFF, purified the live cells, stimulated the BAFF-starved B cells with recombinant BAFF protein, and then monitored activation of the Akt signaling pathway by measuring phosphorylation of Akt and one of its downstream signaling targets, S6 ribosomal protein. As shown in Fig. 5 E, phospho-Akt was observed at higher levels in BAFF-starved *Gnaq*$^{-/-}$ CD43$^{neg}$ B cells than in WT CD43$^{neg}$ B cells. After BAFF stimulation, phospho-Akt levels increased more rapidly in the *Gnaq*$^{-/-}$ B cells. This finding was recapitulated when either FOB or MZB cells were analyzed (Fig. 5 E) but was most striking in the *Gnaq*$^{-/-}$ FOB cell subset (Fig. 5 E). Interestingly, although $G_{\alpha q}$ deficiency amplified BAFF-dependent Akt activation in both FOB and MZB cell subsets, phosphorylation of S6 ribosomal protein was equivalent between BAFF-stimulated WT and *Gnaq*$^{-/-}$ FOB cells (Fig. 5 E). However, phospho-S6 levels were constitutively higher in *Gnaq*$^{-/-}$ MZB cells than in WT B cells and were induced to higher levels in the *Gnaq*$^{-/-}$ MZB cells after BAFF stimulation (Fig. 5 E). Together, these data indicate that the Akt prosurvival pathway is constitutively more active in BAFF-deprived *Gnaq*$^{-/-}$ B cells and that *Gnaq*$^{-/-}$ B cells engage this pathway more efficiently than WT B cells after BAFF stimulation.

### *Gnaq*$^{-/-}$ B cells are spontaneously activated in vivo

Because *Gnaq*$^{-/-}$ B cells are more resistant to BAFF deprivation, we postulated that *Gnaq*$^{-/-}$ B cells may survive peripheral tolerance checkpoints that normally eliminate B cells with self-reactivity. If this were true, then *Gnaq*$^{-/-}$ B cells might be activated and responding to self-antigens. To test this hypothesis, we made 50:50 mixed BM chimeras by reconstituting CD45.1$^{+}$ WT recipients with an equal mixture of CD45.1$^{+}$ WT BM and CD45.2$^{+}$ *Gnaq*$^{-/-}$ BM. We isolated cells from spleen, BM, and lung at 3 mo after reconstitution and used FACS to phenotypically characterize the B cells. *Gnaq*$^{-/-}$ B cells from the mixed BM chimeras expressed statistically higher levels of CD80, CD40, and MHC class II than the WT B cells isolated from the same animals (Fig. S4 A). Next, using peanut agglutinin (PNA) and FAS to identify B cells with a germinal center (GC) phenotype (PNA$^{hi}$Fas$^{+}$), we found only a very small proportion of WT B cells with this phenotype in any tissue (Fig. 6, A and B). However, significantly higher proportions of the *Gnaq*$^{-/-}$ B cells from the same animal expressed PNA$^{hi}$Fas$^{+}$ in spleen, lung, and BM (Fig. 6, A and B), suggesting that *Gnaq*$^{-/-}$ B cells make up most of the GCs present in these mice. In support of this conclusion, we identified well defined B cell follicles in the lungs of $G_{\alpha q}$-deficient chimeras, and some of the B cells within these follicles expressed the GC marker GL7 (Fig. S4 B). As these structures are not found in the lungs of naive normal mice (Moyron-Quiroz et al., 2004), the data suggest that *Gnaq*$^{-/-}$ B cells are being activated by endogenous self-ligands.

### Intrinsic defects in *Gnaq*$^{-/-}$ B cells result in the development of autoreactive B cells

To address whether *Gnaq*$^{-/-}$ B cells are self-reactive, we evaluated whether serum Abs from WT and *Gnaq*$^{-/-}$ chimeras were reactive in a standard anti-nuclear Ab (ANA) assay. As expected, none of the serum samples from WT chimeras exhibited ANA reactivity at any time point after reconstitution (Fig. 6 C). In contrast, ~20% of the serum samples from *Gnaq*$^{-/-}$ chimeras were ANA reactive within 2 mo after reconstitution. By 5 mo after reconstitution, 100% of the serum samples from *Gnaq*$^{-/-}$ chimeras were ANA$^{+}$ (Fig. 6 C). Interestingly, we observed that some of the serum samples strongly stained the entire nucleus, whereas others exhibited a more punctate pattern of staining (Fig. S4 C), suggesting that multiple auto-Ags can be recognized by *Gnaq*$^{-/-}$ B cells. Indeed, we also identified significantly higher levels of anti–double-stranded (ds) DNA reactivity in some *Gnaq*$^{-/-}$ chimera serum samples (Fig. 6 D).

To determine whether the development of autoreactive B cells in *Gnaq*$^{-/-}$ chimeras is the result of an intrinsic defect in the *Gnaq*$^{-/-}$ B cells, we lethally irradiated WT Igh$^{a}$ allotype congenic mice and reconstituted them with 50% WT Igh$^{a}$ BM and 50% Igh$^{b}$ *Gnaq*$^{-/-}$ BM (*Gnaq*$^{-/-}$:WT chimera) or with 50% WT Igh$^{a}$ BM + 50% WT Igh$^{b}$ BM (WT:WT chimera; Fig. 6 E). At various time points after reconstitution, we collected serum and peripheral blood cells. As expected, peripheral blood B cells from the WT:WT chimeras were evenly distributed, with ~50% of the B cells expressing an Igh$^{a}$ BCR and the other half expressing Igh$^{b}$ BCRs (Fig. 6 F). In contrast, in the *Gnaq*$^{-/-}$:WT chimeras, the Igh$^{b}$-expressing *Gnaq*$^{-/-}$ B cells outcompeted the Igh$^{a}$-expressing WT B cells and eventually became the dominant B cell population present in the peripheral blood (Fig. 6 G). We next evaluated the serum samples for ANA reactivity using allotypic-specific Abs to detect the ANAs. As expected, neither Igh$^{a}$ nor Igh$^{b}$ Abs from the serum of WT:WT chimeras exhibited ANA reactivity (Fig. 6 H). However, analysis of serum from the *Gnaq*$^{-/-}$:WT chimeras, revealed that the Igh$^{b}$ Abs (derived from the *Gnaq*$^{-/-}$ B cells) efficiently stained the nucleus of HepG2 cells (Fig. 6 H). In contrast, the Igh$^{a}$ Abs (derived from the WT B cells present in the same host) did not stain HepG2 nuclei (Fig. 6 H). Indeed, ANA reactivity of the WT Igh$^{a}$ Abs from the *Gnaq*$^{-/-}$:WT chimeras did not rise above background and was equivalent to that observed for the Igh$^{a}$ Abs from WT:WT chimeras (Fig. 6 I). This was not the result of a lack of Igh$^{a}$ Ab in the *Gnaq*$^{-/-}$:WT serum samples, as nonautoreactive Igh$^{a}$ Abs were present at low, but still detectable, levels in

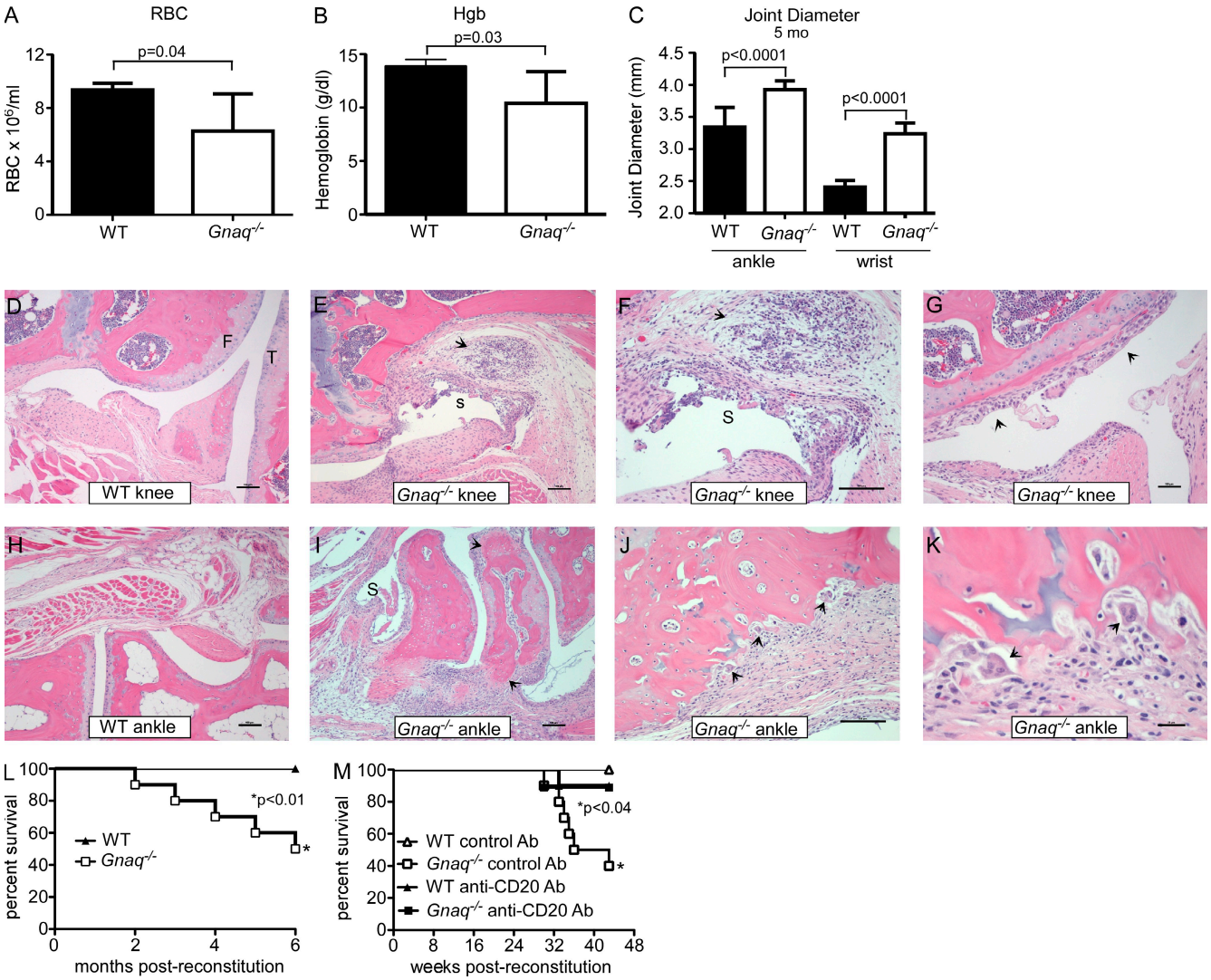


**Figure 7. $G_{\alpha q}$-deficient chimeras develop B cell–dependent systemic autoimmunity.** (A and B) Arterial blood from WT and *Gnaq*$^{-/-}$ BM chimeras (8 mo after reconstitution) was isolated and complete blood cell counts were performed. Mean red blood cell counts (A) and hemoglobin concentration (B) are reported. Data shown are the mean ± SD of four mice/group and are representative of two independent experiments. P-values were determined using an unpaired Student's *t* test. (C) The diameters of ankle and wrist joints were measured in WT and *Gnaq*$^{-/-}$ chimeras at 5 mo after reconstitution. Data are represented as the mean ± SD of 8–10 mice/group. Similar results were seen in three experiments. P-values were determined using an unpaired Student's *t* test. (D–K) Histological analysis (hematoxylin and eosin [H&E]) of knee and ankle joints from WT and *Gnaq*$^{-/-}$ chimeras was performed at 5 mo after reconstitution. (D) Normal knee joint from a WT chimera showing femur (F) and Tibia (T). (E) Knee joint from a *Gnaq*$^{-/-}$ chimera with focal soft tissue inflammation (arrow) adjacent to a joint space (S) where the synovial lining is disrupted. A higher power view (F) demonstrates a focus of mixed inflammatory cells (arrow) and necrosis of the overlying synovium. (G) The articular surface of the distal femur of a *Gnaq*$^{-/-}$ chimera is irregular, thinned, and covered by fibrous pannus (arrows). (H) Normal ankle joint from a WT chimera. (I) Ankle from a *Gnaq*$^{-/-}$ chimera with marked inflammation of soft tissues accompanied by exostotic bone (arrows) and accumulation of fibrin within the joint space (S). (J) Bone from the foot of a *Gnaq*$^{-/-}$ chimera with proliferative periostitis overlying an area of bone lysis represented as scalloping of the bone surface (arrows). (K) Higher power of bone from the foot shows multinucleated osteoclasts within resorptive foci (arrows). Images are from one representative animal out of 5–10 mice/group. Bars: (D–J) 100 µm; (K) 20 µm. Two independent experiments were performed. (L) Survival of *Gnaq*$^{-/-}$ and WT chimeras was tracked for 6 mo after BM reconstitution. Data are shown as the percentage of survival of each group ($n$ = 10 mice/group). P-values were determined using the Wilcoxon test. Data are representative of three independent experiments. (M) $G_{\alpha q}$-deficient and WT chimeras were treated with anti-CD20 (clone 18B12) or control Ab at 2 mo after reconstitution and survival was tracked over the next 11 mo. The experiment was performed once with 10 mice/group. P-values were determined using a Log-rank test.

the *Gnaq*$^{-/-}$:WT chimera serum samples (Fig. S4 D). Together, the data indicate that the development of autoreactive B cells is dependent on the loss of $G_{\alpha q}$ expression in B cells. Furthermore, the loss of $G_{\alpha q}$ in other hematopoietic cells is not sufficient to drive normal B cells to become autoreactive.

### $G_{\alpha q}$ suppresses the development of systemic autoimmunity

Given the propensity of *Gnaq*$^{-/-}$ B cells to secrete autoreactive Abs, we predicted that *Gnaq*$^{-/-}$ chimeras would develop autoimmune disease. To test this, we determined whether immune complexes were present in the kidneys of WT and *Gnaq*$^{-/-}$

chimeras. No Ab-containing immune complexes were detected in the WT kidney sections (Fig. S5, A–C). In contrast, IgG2a- and IgG2c-containing immune complexes were reproducibly observed in kidney sections from *Gnaq*$^{-/-}$ chimeras (Fig. S5, D–F). However, despite immune complex deposition in the kidney, kidney function, as assessed by measuring protein concentration in the urine, was normal in the *Gnaq*$^{-/-}$ chimeras (unpublished data). Histopathologic analysis of the kidneys from *Gnaq*$^{-/-}$ chimeras showed mild to moderate mesangiolysis (thrombotic microangiopathy) with splitting of the basement membranes in the glomeruli and increased mesangial matrix within the glomeruli (Fig. S5, G–J). Although this pathology is atypical for the most common forms of immune complex–mediated disease, thrombotic microangiopathy can be a manifestation of disease in Lupus patients with anti-coagulant, anti-phospholipid, or anti-endothelial Abs (Tektonidou, 2009).

In addition to changes in the kidney, the chimeras exhibited other symptoms consistent with autoimmune disease. For example, we noted that the BM from the older *Gnaq*$^{-/-}$ chimeras appeared to have reduced numbers of RBCs. To test whether the *Gnaq*$^{-/-}$ chimeras develop anemia, we performed complete blood counts on arterial blood from WT and *Gnaq*$^{-/-}$ chimeras. We found that the number of RBCs and the concentration of hemoglobin were significantly reduced in the *Gnaq*$^{-/-}$ chimeras (Fig. 7, A and B). These symptoms are consistent with a diagnosis of autoimmune hemolytic anemia as a result of the presence of anti-RBC Abs, or they could also be a consequence of the autoimmune kidney thrombotic microangiopathy (Tektonidou, 2009).

We also monitored joint swelling in WT and *Gnaq*$^{-/-}$ chimeras, as we observed that many of the older *Gnaq*$^{-/-}$ chimeras were less mobile than their WT counterparts. Significant differences in the size of the joints of *Gnaq*$^{-/-}$ chimeras was observed within 3.5 mo of reconstitution and the penetrance of disease in the *Gnaq*$^{-/-}$ chimeras was 100% (unpublished data). By 5 mo after reconstitution, significant swelling was observed in both ankle and wrist joints of *Gnaq*$^{-/-}$ chimeras compared with the WT chimeras (Fig. 7 C). Histological analysis of knees, ankles, and portions of feet from *Gnaq*$^{-/-}$ chimeras revealed a variety of arthritic changes including chronic/active areas of inflammation within the joints, evidence of synovitis and bone resorption, exostotic bone development, and osteolytic activity (Fig. 7, D–K).

Collectively, our data suggest that *Gnaq*$^{-/-}$ chimeras develop systemic autoimmune disease with multiorgan involvement. Consistent with this, we noted a significant difference between the survival of *Gnaq*$^{-/-}$ and WT chimeras with up to 50% of the *Gnaq*$^{-/-}$ chimeras dying within 6 mo of reconstitution (Fig. 7 L). To test whether the loss of $G_{\alpha q}$ in B cells is responsible for the increased mortality observed in the *Gnaq*$^{-/-}$ chimeras, we depleted B cells in WT and *Gnaq*$^{-/-}$ chimeras at 8 wk after reconstitution using anti–mouse CD20 (Hamel et al., 2008; Yu et al., 2008). We then monitored survival in the anti-CD20 and control Ab–treated chimeras over the next several months. As expected, mortality rates were very low in WT chimeras treated with a single dose of control or anti-CD20 Ab (Fig. 7 M). *Gnaq*$^{-/-}$ chimeras treated with the control Ab had high rates of mortality, with 60% of the chimeras dying within 10 mo of reconstitution (Fig. 7 M). In striking contrast, only 10% of the anti-CD20–treated *Gnaq*$^{-/-}$ chimeras died during the study (Fig. 7 M). Thus, $G_{\alpha q}$ expression by B cells is necessary for normal peripheral B cell development and tolerance induction and also plays a role in preventing early onset mortality in mice.

## DISCUSSION

It is estimated that >800 seven-transmembrane GPCRs are encoded in the mammalian genome. B lymphocytes, like other hematopoietic cells, express GPCRs, some of which play important roles in regulating B lymphocyte adhesion and trafficking (Wettschureck et al., 2004). In this paper, we show that $G_{\alpha q}$ regulates B cell repertoire selection by controlling B cell survival during transitional cell differentiation. Aberrant regulation at this point allows inappropriate survival of autoreactive B cells, ultimately resulting in the development of autoimmune disease.

$G_{\alpha q}$ is expressed in B lineage cells throughout development (Wilkie et al., 1991). However, $G_{\alpha q}$ appears to have little to no effect on the survival or expansion of BM B cell progenitors. Instead, $G_{\alpha q}$ exerts its effects at the earliest T1 stage of transitional B cell development and extends its influence to all transitional and mature B cells subsets. Interestingly, the loss of $G_{\alpha q}$ particularly favors the development of MZB-like cells. At least three precursors for the mature MZB cells have been identified: the T2 MZB precursor (Srivastava et al., 2005), the T1-MZB precursor (Carey et al., 2008), and the FOII precursor (Cariappa et al., 2007). Interestingly, only the T1-MZB precursor population was expanded in the *Gnaq*$^{-/-}$ chimeras and this population was the most highly skewed in favor of *Gnaq*$^{-/-}$ B cells in the mixed BM chimeras. Therefore, we think it likely that the *Gnaq*$^{-/-}$ MZB-like cells develop directly from the T1 MZB precursors.

The MZB compartment contains B cells that are positively selected from a subpopulation of proliferating T2 B cells (Meyer-Bahlburg et al., 2008) as well as potentially autoreactive B cells that escape deletion at the T1 to T2 checkpoint (Thien et al., 2004). T1 B cells with low affinity for self-antigens normally up-regulate BAFFR, colonize the B cell niches of the spleen, and enter the mature B cell pool (Thien et al., 2004). In contrast, B cells of intermediate affinity for self-antigen are excluded from the splenic niches and rapidly die (Cyster et al., 1994). However, when BAFF is readily available, the intermediate affinity autoreactive B cells are rescued and positively selected into the MZ compartment (Thien et al., 2004). These results indicate that B cells with a higher affinity for self-antigen compete less effectively than the lower affinity B cells for a limiting pool of BAFF. It is clear from our data that the *Gnaq*$^{-/-}$ B cells can outcompete WT B cells under homeostatic conditions and that *Gnaq*$^{-/-}$ B cells are less dependent on BAFF for survival than WT B cells. This would permit relaxed stringency of negative selection for the *Gnaq*$^{-/-}$ B cells and allow for the entry of potentially autoreactive cells into the mature MZB compartment. However, it

is important to note that the T1 compartment, which is initially BAFF unresponsive, is also substantially expanded in the *Gnaq*$^{-/-}$ chimeras. Thus, either the loss of $G_{\alpha q}$ affects more than just BAFF responsiveness or a proportion of the T1 cells can become BAFF responsive as they transit this developmental window. Regardless, our combined data strongly imply that loss of $G_{\alpha q}$ facilitates the inappropriate survival of B cells in the periphery.

The data presented in this paper suggests that $G_{\alpha q}$ is an important regulator of B cell homeostasis and survival. Although the neuronal defects in *Gnaq*$^{-/-}$ mice make it impractical for us to monitor the long-term development of clinical autoimmunity without generating BM chimeras, B cell homeostasis was identical in the *Gnaq*$^{-/-}$ mice and the *Gnaq*$^{-/-}$ chimeras. Therefore, our results are not an aberrant manifestation of irradiation and reconstitution but are a result of the loss of $G_{\alpha q}$ specifically in hematopoietic cells. In addition, our data strongly argue that the *Gnaq*$^{-/-}$ B cells are intrinsically defective and are more resistant than the WT B cells to cell death–inducing signals such as BAFF withdrawal or strong BCR signals. Although we do not yet know all the mechanistic details surrounding $G_{\alpha q}$-mediated suppression of B cell survival, we do know that unstimulated and BCR- or BAFF-activated *Gnaq*$^{-/-}$ B cells have higher levels of active Akt as measured by phosphorylation of Ser473, a phosphorylation site which is under PI3K control. Prior work studying fibroblast cell lines (Bommakanti et al., 2000; Ballou et al., 2003) and cardiomyocytes (Howes et al., 2003) showed that $G_{\alpha q}$ normally represses Akt activation. Furthermore, overexpression of $G_{\alpha q}$ in cardiomyocytes leads to cardiac hypertrophy as well as cardiomyocyte apoptosis (Adams et al., 1998). Based on these data, it is speculated that low-level $G_{\alpha q}$ activity may lead to PI3K-dependent Akt activation and cell survival, whereas high or sustained $G_{\alpha q}$ activity results in PI3K/Akt repression and cell death (Hubbard and Hepler, 2006).

Although the active GTP-bound form of $G_{\alpha q}$ interacts with different signaling partners, including PLC-β and Btk (Hubbard and Hepler, 2006), published data indicate that $G_{\alpha q}$ mediates its pro-apoptotic effect in myocytes by binding to p110α and suppressing the production of PIP3 by PI3K (Bommakanti et al., 2000; Ballou et al., 2003). This $G_{\alpha q}$-dependent inhibition of PI3K activity leads to reductions in Akt activation and suppression of the prosurvival mTOR pathway (Manning and Cantley, 2007). Interestingly, expression of activated p110α in B lymphocytes is sufficient to ensure survival of the mature B cell population, even when the BCR has been deleted (Srinivasan et al., 2009). Furthermore, deletion of PTEN, an inhibitor of PI3K, also promotes mature B cell survival (Srinivasan et al., 2009) and can rescue autoreactive B cells from anergy (Browne et al., 2009). Interestingly, the autoreactive prone MZB cell compartment is also expanded in mice expressing activated p110α or lacking PTEN (Anzelon et al., 2003; Srinivasan et al., 2009). Finally, B cells isolated from multiple models of autoimmunity are reported to express elevated levels of phospho-Akt (Wu and Mohan, 2009), and perturbations in the PI3K/Akt axis can lead to the development of autoimmunity (Wu and Mohan, 2009). Based on these data, we speculate that the loss of $G_{\alpha q}$ in B cells leads to increased active PI3K, resulting in the augmented phosphorylation of Akt, activation of the mTOR pathway, and an increase in the MZB compartment. Our experiments indicate that the increased Akt activity observed after BCR engagement is most pronounced in the MZ-like B cells found in *Gnaq*$^{-/-}$ chimeras. This selective enhanced engagement of the prosurvival Akt pathway may explain why these MZB cells are present in larger numbers in the *Gnaq*$^{-/-}$ chimeras. Interestingly, activation of Akt was very similar in the anti-IgM–stimulated FOB cells from *Gnaq*$^{-/-}$ and WT chimeras. This result was initially unexpected given that both MZB and FOB cell subsets are expanded in the *Gnaq*$^{-/-}$ mice. However, Akt is also constitutively more activated in BAFF-deprived *Gnaq*$^{-/-}$ B cells and is increased more strongly after BAFF stimulation. This enhanced response to BAFF was observed in both the FOB and MZB cells from *Gnaq*$^{-/-}$ chimeras. Furthermore, BAFF-induced phosphorylation of S6, a downstream target of the Akt–mTOR pathway, was evident in both the MZB and FOB subsets, although it was most affected in the *Gnaq*$^{-/-}$ MZB cells. Collectively, these data suggest that $G_{\alpha q}$ deficiency confers both FOB and MZB cells with an enhanced ability to activate the PI3K–Akt pathway.

Although we have made progress in identifying the prosurvival signaling pathway that is normally suppressed by $G_{\alpha q}$, we do not yet know which GPCR or ligand mediates this dampening signal in peripheral B cells. Our preliminary transcriptome analysis indicated that >100 different GPCRs, including chemokine receptors, are expressed by mature B cells. Our data suggest that B cell chemotaxis to CXCR4, CXCR5, Edg1, and CCR7 ligands is not abrogated by the loss of $G_{\alpha q}$. Although these data do not exclude the possibility that chemokine receptors play a separate $G_{\alpha q}$-dependent role in regulating B cell survival, it is equally likely that one of the many non-chemokine receptor GPCRs expressed by B cells regulates B cell survival. Unfortunately, surprisingly little is known regarding the role for these other GPCRs in B cells and more work will be needed to evaluate their potential roles in B cell development and selection.

The autoimmune disease that develops in *Gnaq*$^{-/-}$ chimeras is similar, but not identical, to the disease that develops in BAFF Tg mice (Mackay et al., 1999). For example, both strains of mice have increased numbers of MZB cells, develop auto-Abs, and exhibit signs of lupus-like disease. However, kidney failure did not occur in *Gnaq*$^{-/-}$ chimeras, despite evidence of immune complex deposition and mesangiolysis. Instead, the *Gnaq*$^{-/-}$ chimeras develop arthritis and become anemic. Furthermore, the *Gnaq*$^{-/-}$ chimeras develop inflammatory lesions and ectopic lymphoid tissues in multiple organs, including the lung. Given the speed with which autoimmune disease manifests in the *Gnaq*$^{-/-}$ chimeras and the number of affected tissues, we believe that the animals suffer from a widespread autoimmune syndrome that affects multiple organ systems and likely involves autoreactive B cells of different specificities. Importantly, the increased mortality observed in *Gnaq*$^{-/-}$ chimeras is dependent on B cells, as a single round of B cell depletion significantly delayed the onset of morbidity and mortality. Although we do not yet know

whether $G_{\alpha q}$ deficiency in B cells alone is sufficient to induce autoimmune disease, we do know that the loss of $G_{\alpha q}$ specifically within B lineage cells is required for the development and survival of the autoreactive B cells. Together, our results indicate that the loss of $G_{\alpha q}$ in other hematopoietic lineage cells, including T cells, is not sufficient to drive the selection of normal B cells into the autoimmune repertoire.

Although *Gnaq*$^{-/-}$ T cells are not sufficient to induce B cell autoreactivity, we cannot exclude the possibility that *Gnaq*$^{-/-}$ T cells contribute to the disease. Indeed, the presence of GCs containing *Gnaq*$^{-/-}$ B cells in the spleen, lung, LNs, and BM suggests that autoantigen-specific T cells are present and able to drive the GC reaction. Interestingly, a recent publication reported that $G_{\alpha q}$ regulates TCR signaling (Ngai et al., 2008). Preliminary unpublished experiments from our group indicate that *Gnaq*$^{-/-}$ T cells outcompete normal T cells in the thymus of mixed BM chimeras. The competitive advantage of *Gnaq*$^{-/-}$ T cells is observed at the double-negative stage of thymocyte development and persists throughout thymic and peripheral T cell development. However, the *Gnaq*$^{-/-}$ T cells found in the LNs and spleen of the mixed chimeras are not constitutively activated as measured by expression levels of CD44, CD62L, or CD25. Thus, although $G_{\alpha q}$ plays a role in T cell development, it is still not clear whether the loss of $G_{\alpha q}$ expression on T cells will be necessary for the initiation of the autoimmune disorders observed in the *Gnaq*$^{-/-}$ chimeras.

In conclusion, our work illustrates a critical intrinsic role for $G_{\alpha q}$ in the maintenance of peripheral B cell immunological tolerance and shows that deficiencies in $G_{\alpha q}$ expression contribute to the development of autoimmune disease. These data also provide the first demonstration that the survival and selection of B cells into the mature B cell repertoire is not only dependent on NF-κB activation in response to BCR and BAFFR engagement but is also controlled by G protein signals.

## MATERIALS AND METHODS

**Mice, BM chimeras, and in vivo Ab treatments.** All experimental procedures involving mice were approved by the Trudeau Institute Institutional Animal Care and Use Committee (IACUC) and the University of Rochester Committee on Animal Resources. C57BL/6J (B6), *Gnaq*$^{-/-}$ ($n > 5$ backcross to C57BL/6J), CD45.1$^+$ congenic B6, and B6.Cg-Igha Thy1a Ptrpca Pep3b/Boy (Igh$^a$) mice were bred in the University of Rochester or Trudeau Institute animal facilities. BM chimeras were generated by irradiating recipient mice with a split dose of 950 Rads from a $^{137}$Cs irradiator and then reconstituting the recipients with 1–2.5 × 10$^6$ BM cells from B6 or *Gnaq*$^{-/-}$ donors. In some experiments, CD45.1$^+$ recipients were reconstituted with a mixture of 50% WT and 50% *Gnaq*$^{-/-}$ BM (50:50 chimeras). In other experiments, BAFF was depleted by injecting 50:50 BM chimeras i.p. with 250 μg of anti–mouse BAFF/BLyS (clone 10F4; Human Genome Sciences) or control hamster IgG (BioExpress) in PBS 1 time at 8 wk after reconstitution. CD20$^+$ B cells were depleted by injecting *Gnaq*$^{-/-}$ and WT chimeras i.p. with 200 μg of mouse anti–mouse CD20 (clone 18B12 IgG2a; Hamel et al., 2008) or with an isotype control Ab (clone 2B8) one time at 9 wk after reconstitution. B cell–depleted and nondepleted chimeras were monitored for health and survival. Mice that appeared hunched with ruffled fur and/or had difficulty moving were euthanized in accordance with IACUC guidelines.

**Flow cytometry and EdU assays.** B220 APC-AF750 and CD23-APC were obtained from Invitrogen. SA–Pacific orange, SA-APC-AF750, and λ5-AF488 were purchased from Invitrogen. CD19 Pacific blue, CD93 biotin, anti-BAFFR-AF647, and CD45.2-APC-AF750 were produced by eBioscience, and IA/IE Pacific Blue and CD80-AF647 were obtained from BioLegend. All other Abs were purchased from BD. To analyze in vivo cell proliferation, chimeras were injected i.p. twice with the nucleic acid homologue EdU (Invitrogen) 18 h before harvest. Splenocytes were then stained with Abs to CD19 and CD45.2, fixed with 1% neutral buffered formalin, permeabilized with saponin-based buffer, and incubated with the manufacturer-provided Pacific blue–conjugated EdU detection agent. Flow cytometry data were collected using FACSCalibur, Canto II, or LSR II instruments (BD) from the University of Rochester Flow Cytometry Core and were analyzed using FlowJo (Tree Star, Inc.).

**Chemotaxis assays.** Spleen cells from 50:50 mixed BM chimeras were isolated and stained with Abs to B220 and CD45.2 to identify WT (CD45.2$^{neg}$) and *Gnaq*$^{-/-}$ (CD45.2$^+$) B cells. 3 × 10$^5$ total spleen cells were added to the top well of a transwell with a 5-μm pore size polycarbonate filter (Costar), and the indicated amount of chemokine was added to the bottom well. Cells were recovered from the bottom well 2 h later, fixed, and then analyzed and counted on a flow cytometer to determine the number of B cells of each genotype that migrated to the bottom of the transwell. Data are reported as the chemotaxis index, which represents the fold change in the number of cells that migrated in response to the chemokine versus the number of cells that spontaneously migrated in the absence of chemokine. S1P was purchased from Avanti Polar Lipids and CXCL12, CXCL13, and CCL19 were purchased from R&D Systems.

**In vivo B cell migration assay.** B cells were purified from the spleens of CD45.2$^+$ *Gnaq*$^{-/-}$ and CD45.1$^+$ WT chimeras by negative selection (>90% purity) using Abs to CD3, CD11b, and GR1 (MACS; Miltenyi Biotec). WT B cells were incubated at room temperature for 15 min in a solution of 80 μg/ml biotin in PBS. *Gnaq*$^{-/-}$ B cells were incubated at room temperature in PBS only. Cells were washed three times in PBS, resuspended in FACs buffer, and counted. The cells were mixed at a 1:1 ratio and the volume was adjusted to 5 × 10$^7$ cells/ml. CD45.1$^+$ recipient B6 mice ($n = 4$ mice) were then injected i.v. with the cell mixture (10$^7$ cells/recipient). Spleens from the recipient mice were harvested 18 h later and frozen sections were prepared. Sections were stained with PE-labeled anti-CD45.2 (to detect transferred *Gnaq*$^{-/-}$ B cells) and a rat anti–mouse Ab to MOMA-1 (to identify the MZ). Sections were washed and then stained with SA-488 to detect transferred biotinylated WT B cells and an Alexa Fluor 647–labeled anti–rat Ab to detect the MOMA-1$^+$ cells. Slides were viewed on a fluorescent microscope (Axio Observer.Z1; Carl Zeiss, Inc.) using a 10× objective (for 100× total magnification). Images were collected using AxioVision 4.5 software and converted into TIFFs.

**B cell purification and in vitro proliferation and survival assays.** Total B cells were purified by either positive (CD19$^+$) or negative (CD3, CD4, CD8, CD43, CD11b, and CD11c negative) selection by MACS (Miltenyi Biotec). T1 and T2/T3 B cells were sort purified using a FACSAria sorter in the University of Rochester Flow Cytometry Core. Purity of the B cells was >90% in all experiments. To measure proliferation, purified B cells (5 × 10$^5$/ml) were cultured in complete media for 2 d with 0–25 μg/ml of polyclonal goat anti–mouse anti-IgM F(ab′)$_2$ (SouthernBiotech), 0–40 μg/ml of monoclonal rat anti–mouse CD40 (clone 1C10), or 0–10 μg/ml LPS (*Escherichia coli* 055:B5) followed by the addition of 1 μCi 3H-thymidine for 5 h. Thymidine incorporation was measured using a scintillation counter. For in vitro survival experiments, 10$^6$ B cells/ml were cultured in media alone or were stimulated with 10–15 μg/ml of anti-IgM F(ab′)$_2$. Cells from the cultures were collected at 18–24 h and stained with propidium iodide to determine the percentage of live cells.

**B cell transfers.** Splenic B cells from WT and *Gnaq*$^{-/-}$ chimeras (both CD45.2$^+$) were purified by positive selection using MACS. 2.5 × 10$^7$ donor B cells were transferred i.v. into individual CD45.1$^+$ hosts. Spleens from host mice were isolated at 7, 14, and 21 d after transfer and the percentage and total number of transferred donor B cells were determined using flow cytometry.

**Western blot analysis.** Total naive B cells were purified (negative selection with biotinylated CD4, CD8, CD11c, and F4/80 Abs and SA microbeads or anti-CD43 beads; Miltenyi Biotec). CD43$^{neg}$ B cells were further separated

using biotinylated mouse anti-CD21/35 (eBioscience) and SA microbeads (Miltenyi Biotec). The cells not retained on the column were highly enriched for FOB ($CD23^{hi}CD21^{lo}$), whereas the B cells retained on the column were enriched for MZB as defined by CD21/CD23 and CD1d staining. The enrichment of FOB and MZB cells was equivalent between the $Gnaq^{-/-}$ and WT groups, allowing for direct comparison between the groups.

After isolation, B cells were rested for 1 h in RPMI at 37°C before stimulation with 20 μg/ml anti-IgM $F(ab')_2$ ($8 \times 10^6$ B cells per time point). Alternatively, for BAFF stimulations, B cells were cultured overnight in the absence of BAFF in RPMI supplemented with 10% FBS, 2 mM L-glutamine, 50 μM 2-ME, and antibiotics. Viable cells were then isolated by centrifugation using 1-step Polymorph gradients (Accurate Chemical & Scientific Corporation). Cells were washed with unsupplemented RPMI and rested for 1 h at 37°C before stimulation with 25 ng/ml BAFF (R&D Systems) in RPMI for the indicated times. B cells were lysed after stimulation in 1% NP-40 lysis buffer containing protease inhibitors. Cell lysates were recovered and frozen at −70°C until used. For Western blotting assays, $4 \times 10^6$ cell equivalents per lane were resolved on 8% SDS-PAGE gels and transferred to PVDF membranes. Membranes were blocked and then probed with Abs specific for total phosphotyrosine (clone 4G10; Millipore), total phospho-Serine PKC substrates, phospho-Akt, total Akt, and phospho-S6 ribosomal protein (Cell Signaling Technology), phospho-ERK, ERK, and PLCγ2 (Santa Cruz Biotechnology, Inc.) or phospho-Y759 of mouse PLCγ2 (Humphries et al., 2004). Membranes were washed and then incubated with anti–rabbit IgG IRDye800 (Rockland Immunochemicals) or anti–mouse IgG Alexa Fluor 680 (Invitrogen). Proteins were detected and quantified by Infrared Imaging System (LI-COR Biosciences). Gel images were captured using the Gel-Doc It Imaging System (UVP) and the GelCam310 charge-coupled device camera and Visionworks LS software. Gamma settings, background, and contrast were not adjusted.

**ANA analysis.** Serum was diluted 1:100 in PBS/0.2% BSA and incubated on slides with acetone-fixed HepG2 cells. Slides were washed and stained with anti–mouse IgG FITC (SouthernBiotech). In some experiments, biotinylated allotype-specific Abs (recognizing $Igh^a$ or $Igh^b$ Abs; BD) were used to detect the $ANA^+$ Abs in the serum samples. The allotype-specific detection Abs were then visualized using SA-AF488. Slides were mounted with Aqua PolyMount and analyzed on a fluorescent microscope (Axio Observer. Z1) using a Plan-Apochromat 20×/0.8 M27 objective. Images were acquired using a camera (1394 ORCA-ERA; Hamamatsu Photonics) with exposure times ranging from 150 to 400 μs. Data were collected using AxioVision Rel 4.7 software and then converted to TIFF files.

**ELISAs.** To detect circulating total $Igh^a$ or $Igh^b$ Ab in serum from 50:50 mixed BM chimeras, serum was diluted 1:2,700 in PBS and used to coat ELISA plates. Plates were then probed with biotinylated allotype-specific Abs that could distinguish $Igh^a$ and $Igh^b$ Abs from one another (BD). The allotype-specific detection Abs were visualized using SA-HRP (SouthernBiotech). To detect anti-dsDNA Abs, 96-well Immuno Plates (Thermo Fisher Scientific) were coated with 0.01% poly-L-lysine solution in PBS (Sigma-Aldrich) followed by 100 μg/ml deoxyribonucleic acid (Sigma-Aldrich). After blocking, serum samples, diluted 1:200 in 0.05% Tween 20/0.5% BSA/PBS, were added. Plates were washed and then developed with goat anti–mouse IgG HRP (SBA). The OD readings from three wells were averaged for each serum sample.

**Complete blood counts.** Whole blood from the descending aorta of freshly euthanized mice was collected using a tuberculin syringe. Blood was added to EDTA coated Vacutainer tubes (BD) and was counted on a HESKA Veterinary Hematology System, according to manufacturer's instructions.

**Joint pathology.** Wrists and ankles of $Gnaq^{-/-}$ and WT chimeras were measured using digital calipers every 2 wk beginning at 4 wk after reconstitution. To assess pathological changes to the joints, chimeras were euthanized and dissected at 5 mo after reconstitution. The carcasses were fixed in 10% neutral buffered formalin (Sigma-Aldrich). Skeletal tissues were decalcified in a formic acid solution (Cal-Rite; Thermo Fisher Scientific), embedded in paraffin, and cut on a microtome (6-μm sections). Sections were stained with H&E and evaluated by a board-certified veterinary pathologist who was blinded to the experimental design. Images were collected using a microscope (Eclipse 80i; Nikon) with Plan Fluro 10×/0.30, Plan Fluro 20×/0.50, and Plan Fluro 60×/0.85 objectives. Images were recorded with a Digital Sight D5-5M camera using NIS Elements Acquisition Software (Nikon). Postimage processing was performed with NIS Elements for total picture contrast, balance, and color. All changes were made across the entire image and no spot changes were performed.

**Immunofluorescence.** Spleens from WT or $Gnaq^{-/-}$ chimeras were harvested in OCT buffer (Tissue-Tek), snap frozen in $LN_2$, sectioned (5 μm) on a cryostat, and then stained with anti-B220 Alexa Fluor 488, anti-CD21 Alexa Fluor 594, and anti-CD90.2 biotin followed by SA–Alexa Fluor 350. Slides were mounted in PolyMount fluorescent mounting media and viewed on an Axio Observer.Z1 fluorescent microscope at 100× (10× objective lens) using AxioVision 4.5 software. Images were converted to TIFFs and postprocessing imaging was performed in Canvas. Minor adjustments to brightness were performed equally across the whole image.

**Online supplemental material.** Fig. S1 shows FACS analysis of WT and $G_{\alpha q}$-deficient B cell development in BM and spleen. Fig. S2 shows that BCR ligation of $G_{\alpha q}$-deficient B cells leads to elevated tyrosine and serine phosphorylation of proteins. Fig. S3 shows that increased resistance of $G_{\alpha q}$-deficient B cells to BAFF blockade is not a result of altered BAFFR expression. Fig. S4 shows that $G_{\alpha q}$-deficient B cells are activated and display autoreactive specificities. Fig. S5 shows that $G_{\alpha q}$-deficient chimeras develop immune complexes in the kidney and exhibit signs of kidney damage. Online supplemental material is available at http://www.jem.org/cgi/content/full/jem.20092735/DC1.

The authors would like to thank Lizz LaMere and Kyle Martin for management of animal breeding and genotyping and would like to acknowledge the University of Rochester Flow Facility Core for help with sorting and analysis of samples. The authors would also like to thank Randall Rossi and the University of Rochester Wilmot Cancer Center for use of the HESKA Veterinary Hematology System and Dr. Alex Rosenberg for analysis of GPCR mRNA expression levels in naive B cells.

This work was supported by the University of Rochester and National Institutes of Health grants AI068056 to F.E. Lund, F32AI080104 to R.S. Misra, HL69409 to T.D. Randall, HD037091 to D.J. Rawlings, and DK076126 to C.E. Alpers. M. Simon is supported by a Senior Scholar award from the Ellison Medical Foundation and G. Shi is supported by Natural Science Foundation of China grants 30830094 and 30972678.

The authors declare no financial conflicts of interest related to this work.

**Submitted: 22 December 2009**
**Accepted: 17 June 2010**

## REFERENCES

Adams, J.W., Y. Sakata, M.G. Davis, V.P. Sah, Y. Wang, S.B. Liggett, K.R. Chien, J.H. Brown, and G.W. Dorn II. 1998. Enhanced Galphaq signaling: a common pathway mediates cardiac hypertrophy and apoptotic heart failure. *Proc. Natl. Acad. Sci. USA*. 95:10140–10145. doi:10.1073/pnas.95.17.10140

Anzelon, A.N., H. Wu, and R.C. Rickert. 2003. Pten inactivation alters peripheral B lymphocyte fate and reconstitutes CD19 function. *Nat. Immunol.* 4:287–294. doi:10.1038/ni892

Ballou, L.M., H.Y. Lin, G. Fan, Y.P. Jiang, and R.Z. Lin. 2003. Activated G alpha q inhibits p110 alpha phosphatidylinositol 3-kinase and Akt. *J. Biol. Chem.* 278:23472–23479. doi:10.1074/jbc.M212232200

Bommakanti, R.K., S. Vinayak, and W.F. Simonds. 2000. Dual regulation of Akt/protein kinase B by heterotrimeric G protein subunits. *J. Biol. Chem.* 275:38870–38876. doi:10.1074/jbc.M007403200

Browne, C.D., C.J. Del Nagro, M.H. Cato, H.S. Dengler, and R.C. Rickert. 2009. Suppression of phosphatidylinositol 3,4,5-trisphosphate production is a key determinant of B cell anergy. *Immunity*. 31:749–760. doi:10.1016/j.immuni.2009.08.026

Cancro, M.P. 2009. Signalling crosstalk in B cells: managing worth and need. *Nat. Rev. Immunol.* 9:657–661. doi:10.1038/nri2621

Carey, J.B., C.S. Moffatt-Blue, L.C. Watson, A.L. Gavin, and A.J. Feeney. 2008. Repertoire-based selection into the marginal zone compartment

during B cell development. *J. Exp. Med.* 205:2043–2052. doi:10.1084/jem.20080559

Cariappa, A., C. Boboila, S.T. Moran, H. Liu, H.N. Shi, and S. Pillai. 2007. The recirculating B cell pool contains two functionally distinct, long-lived, posttransitional, follicular B cell populations. *J. Immunol.* 179:2270–2281.

Cyster, J.G., S.B. Hartley, and C.C. Goodnow. 1994. Competition for follicular niches excludes self-reactive cells from the recirculating B-cell repertoire. *Nature.* 371:389–395. doi:10.1038/371389a0

Dalwadi, H., B. Wei, M. Schrage, K. Spicher, T.T. Su, L. Birnbaumer, D.J. Rawlings, and J. Braun. 2003. B cell developmental requirement for the G alpha i2 gene. *J. Immunol.* 170:1707–1715.

Frey, U.H., W. Lieb, J. Erdmann, D. Savidou, G. Heusch, K. Leineweber, H. Jakob, H.W. Hense, H. Löwel, N.H. Brockmeyer, et al. 2008. Characterization of the GNAQ promoter and association of increased Gq expression with cardiac hypertrophy in humans. *Eur. Heart J.* 29:888–897. doi:10.1093/eurheartj/ehm618

Fruman, D.A., and G. Bismuth. 2009. Fine tuning the immune response with PI3K. *Immunol. Rev.* 228:253–272. doi:10.1111/j.1600-065X.2008.00750.x

Goodnow, C.C. 2007. Multistep pathogenesis of autoimmune disease. *Cell.* 130:25–35. doi:10.1016/j.cell.2007.06.033

Hamel, K., P. Doodes, Y. Cao, Y. Wang, J. Martinson, R. Dunn, M.R. Kehry, B. Farkas, and A. Finnegan. 2008. Suppression of proteoglycan-induced arthritis by anti-CD20 B Cell depletion therapy is mediated by reduction in autoantibodies and CD4+ T cell reactivity. *J. Immunol.* 180:4994–5003.

Harris, D.M., A.D. Eckhart, and W.J. Koch. 2006. Galphaq and its Aktions. *J. Mol. Cell. Cardiol.* 40:589–592. doi:10.1016/j.yjmcc.2006.03.001

Howes, A.L., J.F. Arthur, T. Zhang, S. Miyamoto, J.W. Adams, G.W. Dorn II, E.A. Woodcock, and J.H. Brown. 2003. Akt-mediated cardiomyocyte survival pathways are compromised by G alpha q-induced phosphoinositide 4,5-bisphosphate depletion. *J. Biol. Chem.* 278:40343–40351. doi:10.1074/jbc.M305964200

Howes, A.L., S. Miyamoto, J.W. Adams, E.A. Woodcock, and J.H. Brown. 2006. Galphaq expression activates EGFR and induces Akt mediated cardiomyocyte survival: dissociation from Galphaq mediated hypertrophy. *J. Mol. Cell. Cardiol.* 40:597–604. doi:10.1016/j.yjmcc.2005.12.003

Hubbard, K.B., and J.R. Hepler. 2006. Cell signalling diversity of the Gqalpha family of heterotrimeric G proteins. *Cell. Signal.* 18:135–150. doi:10.1016/j.cellsig.2005.08.004

Humphries, L.A., C. Dangelmaier, K. Sommer, K. Kipp, R.M. Kato, N. Griffith, I. Bakman, C.W. Turk, J.L. Daniel, and D.J. Rawlings. 2004. Tec kinases mediate sustained calcium influx via site-specific tyrosine phosphorylation of the phospholipase Cgamma Src homology 2-Src homology 3 linker. *J. Biol. Chem.* 279:37651–37661. doi:10.1074/jbc.M311985200

Lesley, R., Y. Xu, S.L. Kalled, D.M. Hess, S.R. Schwab, H.B. Shu, and J.G. Cyster. 2004. Reduced competitiveness of autoantigen-engaged B cells due to increased dependence on BAFF. *Immunity.* 20:441–453. doi:10.1016/S1074-7613(04)00079-2

Liggett, S.B., R.J. Kelly, R.R. Parekh, S.J. Matkovich, B.J. Benner, H.S. Hahn, F.M. Syed, A.S. Galvez, K.L. Case, N. McGuire, et al. 2007. A functional polymorphism of the Galphaq (GNAQ) gene is associated with accelerated mortality in African-American heart failure. *Hum. Mol. Genet.* 16:2740–2750. doi:10.1093/hmg/ddm229

Lindsley, R.C., M. Thomas, B. Srivastava, and D. Allman. 2007. Generation of peripheral B cells occurs via two spatially and temporally distinct pathways. *Blood.* 109:2521–2528. doi:10.1182/blood-2006-04-018085

Mackay, F., S.A. Woodcock, P. Lawton, C. Ambrose, M. Baetscher, P. Schneider, J. Tschopp, and J.L. Browning. 1999. Mice transgenic for BAFF develop lymphocytic disorders along with autoimmune manifestations. *J. Exp. Med.* 190:1697–1710. doi:10.1084/jem.190.11.1697

Manjarrez-Orduño, N., T.D. Quách, and I. Sanz. 2009. B cells and immunological tolerance. *J. Invest. Dermatol.* 129:278–288. doi:10.1038/jid.2008.240

Manning, B.D., and L.C. Cantley. 2007. AKT/PKB signaling: navigating downstream. *Cell.* 129:1261–1274. doi:10.1016/j.cell.2007.06.009

Meyer-Bahlburg, A., S.F. Andrews, K.O. Yu, S.A. Porcelli, and D.J. Rawlings. 2008. Characterization of a late transitional B cell population highly sensitive to BAFF-mediated homeostatic proliferation. *J. Exp. Med.* 205:155–168. doi:10.1084/jem.20071088

Moyron-Quiroz, J.E., J. Rangel-Moreno, K. Kusser, L. Hartson, F. Sprague, S. Goodrich, D.L. Woodland, F.E. Lund, and T.D. Randall. 2004. Role of inducible bronchus associated lymphoid tissue (iBALT) in respiratory immunity. *Nat. Med.* 10:927–934. doi:10.1038/nm1091

Ngai, J., T. Methi, K.W. Andressen, F.O. Levy, K.M. Torgersen, T. Vang, N. Wettschureck, and K. Taskén. 2008. The heterotrimeric G-protein alpha-subunit Galphaq regulates TCR-mediated immune responses through an Lck-dependent pathway. *Eur. J. Immunol.* 38:3208–3218. doi:10.1002/eji.200838195

Offermanns, S., K. Hashimoto, M. Watanabe, W. Sun, H. Kurihara, R.F. Thompson, Y. Inoue, M. Kano, and M.I. Simon. 1997. Impaired motor coordination and persistent multiple climbing fiber innervation of cerebellar Purkinje cells in mice lacking Galphaq. *Proc. Natl. Acad. Sci. USA.* 94:14089–14094. doi:10.1073/pnas.94.25.14089

Patke, A., I. Mecklenbräuker, H. Erdjument-Bromage, P. Tempst, and A. Tarakhovsky. 2006. BAFF controls B cell metabolic fitness through a PKCβ- and Akt-dependent mechanism. *J. Exp. Med.* 203:2551–2562. doi:10.1084/jem.20060990

Pogue, S.L., T. Kurosaki, J. Bolen, and R. Herbst. 2000. B cell antigen receptor-induced activation of Akt promotes B cell survival and is dependent on Syk kinase. *J. Immunol.* 165:1300–1306.

Shi, G., S. Partida-Sánchez, R.S. Misra, M. Tighe, M.T. Borchers, J.J. Lee, M.I. Simon, and F.E. Lund. 2007. Identification of an alternative $G_{\alpha q}$-dependent chemokine receptor signal transduction pathway in dendritic cells and granulocytes. *J. Exp. Med.* 204:2705–2718. doi:10.1084/jem.20071267

Srinivasan, L., Y. Sasaki, D.P. Calado, B. Zhang, J.H. Paik, R.A. DePinho, J.L. Kutok, J.F. Kearney, K.L. Otipoby, and K. Rajewsky. 2009. PI3 kinase signals BCR-dependent mature B cell survival. *Cell.* 139:573–586. doi:10.1016/j.cell.2009.08.041

Srivastava, B., W.J. Quinn III, K. Hazard, J. Erikson, and D. Allman. 2005. Characterization of marginal zone B cell precursors. *J. Exp. Med.* 202:1225–1234. doi:10.1084/jem.20051038

Stadanlick, J.E., M. Kaileh, F.G. Karnell, J.L. Scholz, J.P. Miller, W.J. Quinn III, R.J. Brezski, L.S. Treml, K.A. Jordan, J.G. Monroe, et al. 2008. Tonic B cell antigen receptor signals supply an NF-kappaB substrate for prosurvival BLyS signaling. *Nat. Immunol.* 9:1379–1387. doi:10.1038/ni.1666

Su, T.T., and D.J. Rawlings. 2002. Transitional B lymphocyte subsets operate as distinct checkpoints in murine splenic B cell development. *J. Immunol.* 168:2101–2110.

Tektonidou, M.G. 2009. Renal involvement in the antiphospholipid syndrome (APS)-APS nephropathy. *Clin. Rev. Allergy Immunol.* 36:131–140. doi:10.1007/s12016-008-8112-z

Thien, M., T.G. Phan, S. Gardam, M. Amesbury, A. Basten, F. Mackay, and R. Brink. 2004. Excess BAFF rescues self-reactive B cells from peripheral deletion and allows them to enter forbidden follicular and marginal zone niches. *Immunity.* 20:785–798. doi:10.1016/j.immuni.2004.05.010

Wettschureck, N., A. Moers, and S. Offermanns. 2004. Mouse models to study G-protein-mediated signaling. *Pharmacol. Ther.* 101:75–89. doi:10.1016/j.pharmthera.2003.10.005

Wilkie, T.M., P.A. Scherle, M.P. Strathmann, V.Z. Slepak, and M.I. Simon. 1991. Characterization of G-protein alpha subunits in the Gq class: expression in murine tissues and in stromal and hematopoietic cell lines. *Proc. Natl. Acad. Sci. USA.* 88:10049–10053. doi:10.1073/pnas.88.22.10049

Wu, T., and C. Mohan. 2009. The AKT axis as a therapeutic target in autoimmune diseases. *Endocr. Metab. Immune Disord. Drug Targets.* 9:145–150. doi:10.2174/187153009788452417

Yanamadala, V., H. Negoro, and B.M. Denker. 2009. Heterotrimeric G proteins and apoptosis: intersecting signaling pathways leading to context dependent phenotypes. *Curr. Mol. Med.* 9:527–545. doi:10.2174/156652409788488784

Yu, S., R. Dunn, M.R. Kehry, and H. Braley-Mullen. 2008. B cell depletion inhibits spontaneous autoimmune thyroiditis in NOD.H-2h4 mice. *J. Immunol.* 180:7706–7713.